PARAMETRIC ANALYSIS OF A DETONATION-TYPE TURBOFAN

by

YASHWANTH M. SWAMY

Presented to the Faculty of the Graduate School of

The University of Texas at Arlington in Partial Fulfillment

of the Requirements

for the Degree of

MASTER OF SCIENCE IN AEROSPACE ENGINEERING

THE UNIVERSITY OF TEXAS AT ARLINGTON

December 2011

ACKNOWLEDGEMENTS

I would like to first thank Dr. Frank Lu for his guidance throughout the project. He has been a constant source of motivation to me and it has been a rich experience to work for him. I would also like to thank Dr. Don Wilson and Dr. Luca Massa for taking time to serve on my committee.

I wish to thank my parents, V M M Swamy and Naveena Swamy, who taught me everything I know and supported me over the years. I would also like to thank my sister and grandparents for their love and support. I dedicate this thesis to my family.

November 8, 2011

ABSTRACT

PARAMETRIC ANALYSIS OF A DETONATION-TYPE TURBOFAN

YASHWANTH M. SWAMY, M.S.

The University of Texas at Arlington, 2011

Supervising Professor: Dr. Frank K. Lu

A new type of turbofan which detonates a fuel-air mixture was theoretically found to perform better than a conventional turbofan. A continuous detonation process is described and considered inside the core of the turbofan. The detonation-type turbofan needs certain modifications to detonate the fuel-air mixture at the core of the turbofan, namely, an annular detonation chamber to achieve continuous detonation. A parametric analysis of the new detonation-type turbofan was developed and used to calculate the performance parameters.

TABLE OF CONTENTS

LIST OF FIGURES

LIST OF TABLES

NOMENCLATURE

a	Size (width) of the self-excited cell of the detonation front (m/in)
u	Velocity of a combustion wave
c	Velocity of sound
d	Mean diameter of the annular chamber
d_c	Diameter of the outer wall of the chamber
G	Total flow rate of the mixture
g	Specific flow rate of the mixture
I_{sp}	Specific impulse
J	Enthalpy
L	Length of the chamber
l	Distance between the two neighboring transverse detonation waves
M	Mach number
P	Pressure
γ	Specific heat ratio
Δ	Distance between the walls of the annular chamber
λ	Total length of the reaction zone
π	Total pressure ratios
ρ	Density
T	Temperature
P	Pressure
D	Detonation wave velocity

α	By-pass ratio
CJ	Chapman-Jouguet

Subscripts

t	Stagnation or total parameters
$0-19$	Station numbers of a standard turbofan
b	Burner

CHAPTER 1

INTRODUCTION

The harnessing of detonations for aero propulsion has gained much interest in the recent past. At present pulse detonation wave engines (PDWEs) and rotating or continuous detonation wave engines (RDWEs or CDWEs) are being researched worldwide, for they may hold a more efficient means of aerospace propulsion. This study is an analysis of an RDWE and means to integrate it into a separate flow turbofan. This study also compares the performance of the detonation-type turbofan with the performance of a standard turbofan.

1.1 Detonation and Deflagration

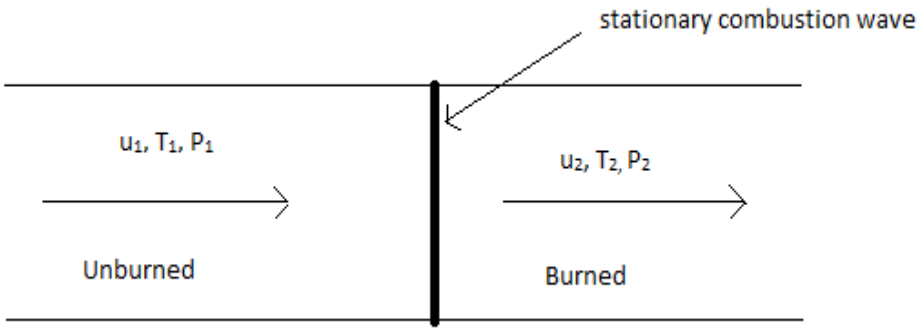

Figure 1 Schematic of a stationary combustion wave.

Detonation and deflagration are the two modes of combustion. Figure 1 depicts a combustion wave travelling through a reactive gaseous mixture in a tube in a reference frame fixed on the wave. In the figure, subscripts 1 and 2 represent the state of unburned gases ahead of the combustion wave and the state of the burned gases behind the combustion wave respectively. Detonations are being currently considered for power generation, air-breathing jet-

engines, rockets and certain other related disciplines .Since detonation itself is preceded by a shock wave which compresses the flow, the actual compression ratio needed by the turbo-machinery is expected to be low in the range of 3-8. Thus, heavy turbo machinery is not expected to be required in detonation-based propulsion systems.

Table 1 Qualitative differences between detonation and deflagration [2]

	Detonation	Deflagration
u_1/c_1	5-10	0.0001-0.03
u_2/u_1	0.4-0.7	4-6
p_2/p_1	13-55(compression)	~0.98(slight expansion)
T_2/T_1	8-21	4-16
ρ_2/ρ_1	1.7-2.6	0.006-0.25

In an ordinary turbofan, combustion of the fuel-air mixture takes place through deflagration. We will see in the present study, how detonation can be utilized instead of deflagration for better efficiency in a turbofan. As seen in table 1, detonation waves heat the reactive gaseous mixture to a higher temperature than its subsonic, deflagration counterpart. Detonation compresses flow whereas deflagration slightly expands the flow as is evident from the table. This can be attributed to the shock wave which always precedes a detonation wave. Also seen is that the ratio of the speed of the unburned gas to local speed of sound (u_1/c_1) is higher in the case of detonation (due to the supersonic nature of the wave) and the ratio of the speeds of burned to unburned gas is lower in detonation waves.

1.2 Outline

The geometry and the various constraints of the geometry of continuously rotating detonation wave concept in an annular chamber [3] are described in section 1.3.The method of analysis is described in section 1.4.

In the process of integration, un-starting of the engine was a primary challenge due to the high pressures developed in the detonation chamber. There might even be a back flow of the combustible mixture or combustion wave which is highly undesirable and potentially disastrous. Thus an “Isolator” is integrated into the system which is expected to address this situation. Brief details about Isolator and its workings are given in section 1.5.

In CDWE, “continuous” means that the detonation, which rotates around an annual chamber, will not cease as long as reactants are fed and the combustion products are removed continuously. Such a detonation chamber is proposed for replacing the ordinary combustion (deflagration) chamber in a turbofan. Since a detonation wave strongly compresses the flow, high pressures are obtained and correspondingly high temperatures, which would require exotic alloys to withstand such extreme conditions. The exhaust enters a turbine (which provides power to the compressor and other systems) and exits into the ambient through an exhaust nozzle. Analysis is performed to explore the performance of such an engine. More details on the analysis are given in chapter 2.

Chapter 3 contains all the assumptions, methods, code descriptions, results, and discussions made.

1.3 Geometry and Modeling

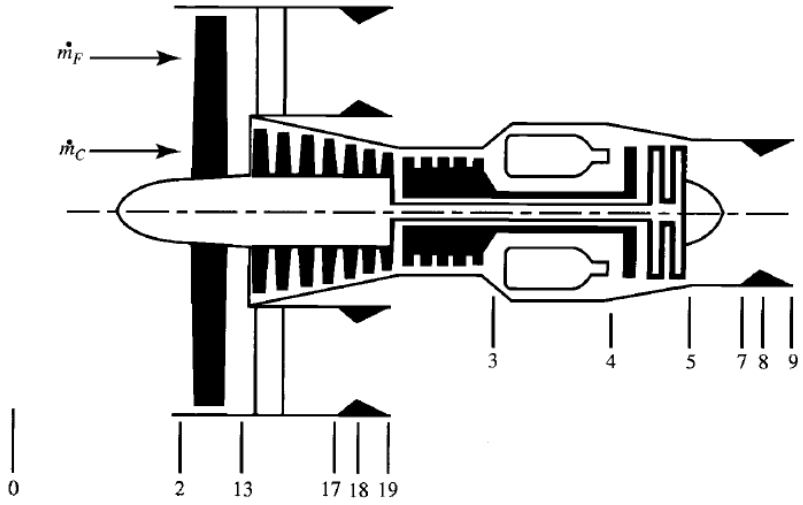

Figure 2 Standard station numbering of a turbofan [1]

Figure 2 shows the standard station numbering of a standard turbofan, stations 0, 2, 3, 4, and 5 correspond to free stream, fan, compressor, combustor, turbine, and exhaust nozzle respectively. Stations 17-19 represent the by-pass. The stream flowing into the core (core flow) and the part of the flow by-passing (secondary flow) are $\dot{m}_c$ and $\dot{m}_f$ respectively. The region between station 4 and station 5, the combustor is the region of interest in this study. An annular detonation chamber as in figure 3 replaces the combustor.

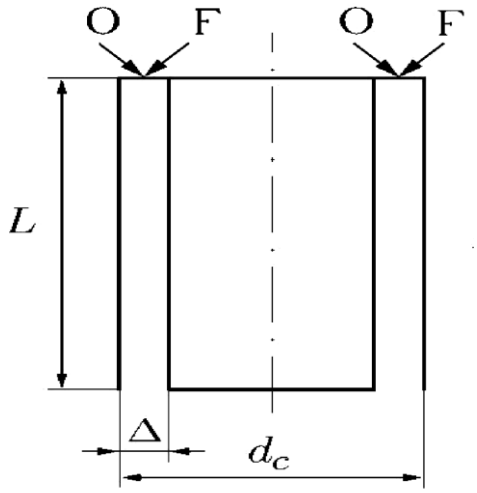

Figure 3 Simple front view of the detonation chamber [3]

Figure 3 is a simple visualization aid of the detonation chamber; where in an explosive gaseous mixture of oxidizer-fuel is injected through a manifold of orifices into an annular chamber of length L with Δ being the distance between the walls of the annular chamber and with an outer diameter d_{c}. The governing factor in obtaining continuous detonation is the mixing in the transverse detonation wave (TDW) front region. Another factor is the renewal of the combustible/explosive mixture ahead of the TDW front. Moreover the height to which this layer is renewed is of importance since there is a certain threshold or critical value h^*, below which the TDW will fade out. The critical value h^* is related to λ, which is the total length of the reaction zone in the detonation wave. [3]

An average relationship is provided by [3]:

$$h \cong h^* \cong (17 \pm 7)\lambda \tag{1}$$

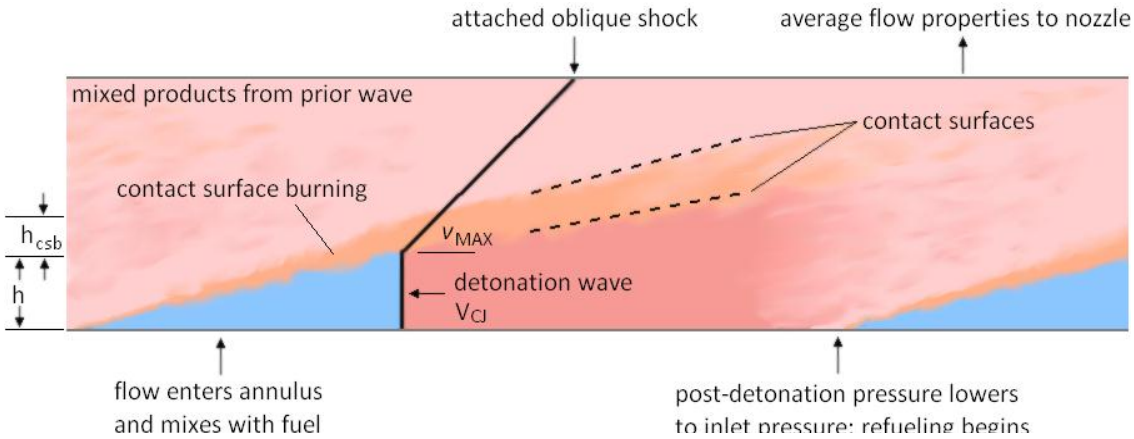

Figure 4 Schematic of the rotating detonation wave structure [7]

Figure 4 shows the rolled out view of the annulus where-in contact burning is shown which has been ignored in the present study to simplify the analysis. The figure also shows a 2D view of the structure of the detonation wave and the attached oblique shock wave.

1.3.1 Description of Geometric Parameters

The value of λ is determined by the time of physical processes for formation of an explosive mixture (fragmentation of drops behind the leading shock wave, evaporation, diffusion, and turbulent mixing of fuel components) and the subsequent time of the chemical reaction. If an ideal case is assumed where in there is a complete pre-mixing, the characteristic chemical length of the zone can be approximated as:

$$\lambda = 0.7a \tag{2}$$

where a is the width of the self-excited cell of the detonation front. The value of a can be determined experimentally in detonation tubes and is known for a large number of mixtures and can also be calculated from known methods provided the physiochemical data; [3, 9]

From (1) and (2) we obtain

$$h = (12 \pm 5)\, a \tag{3}$$

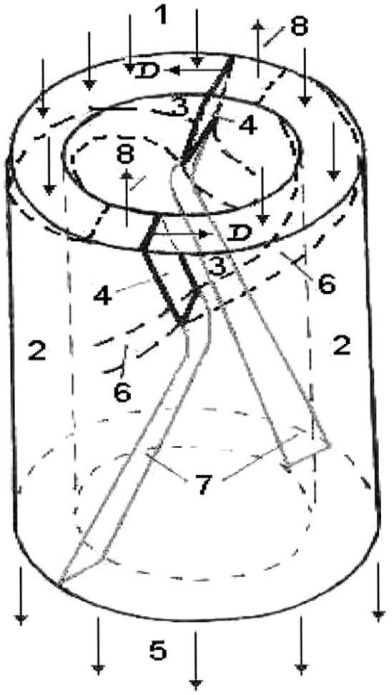

Figure 5 Isometric view of the detonation chamber with categorization [3]

Figure 5 is a schematic of the continuous detonation process in an isometric view, fuel-air mixture (1) are injected into the annular duct (2). Transverse detonation waves (TDW) (4) propagate through the mixture being formed (3). An oblique shock wave (7) is attached to the TDW. Detonation products (5) exit the chamber and due to the high pressure difference some products (8) may enter the injection system. The products and reactants are kept separated by a contact discontinuity (6).

Another important geometric parameter of the process under the discussion is the relation

$$K = \frac{l}{h} = \pi \cdot \frac{d_c}{nh} \tag{4}$$

Experiments [3] reveal that K is roughly a constant for all annular cylindrical chambers involving a gaseous oxidizer and the value being

$$K = 7 \pm 2 \tag{5}$$

Thus, by knowing K we can back calculate the minimum chamber diameter from the previous equation:

$$(d_c)_{\min} = \frac{hK}{\pi} \tag{6}$$

For chambers operating with a gaseous oxidizer, [3]

$$(d_c)_{\min} = 40\lambda \tag{7}$$

The minimum length of the chambers is determined experimentally [3]. It is approximated by the relation

$$L_{\min} = 2h = \frac{d_c}{n} \tag{8}$$

But the continuous detonation process occurring at $L < 3h$ is not efficient enough; it proceeds with incomplete combustion of the fuel. The optimal length is two to three times greater than the minimum length

$$L_{opt} \geq 4h \cong 0.7l \cong \frac{2d_c}{n} \tag{9}$$

The minimum possible radial size can be found from the expression

$$\Delta \geq \Delta^* = 0.2h \tag{10}$$

h is determined by the critical conditions of detonation propagation; the wall friction and heat losses of TDWs.

The data in Table 2 will facilitate the present calculations. [4] Table 2 gives us the numerical values of certain geometrical parameters which are experimentally [3, 5] established and aid us in calculations in section 2.2.2 and 2.2.3.

Table 2 Detonation chamber sizing [4, 5]

Fuel oxidizer combination ($\varphi = 1$)	$\lambda(\mathrm{mm})$	$h(m)$	$d_{\min}(m)$
$2H_2 + Air$	10.9	0.131	0.436

The frequency of the detonation wave is given by:

$$F = \frac{D}{l} = \frac{Dn}{\pi d_c} = \frac{D}{\pi (d_c)_{\min}} \tag{11}$$

1.3.2 Components of a Hybrid Turbofan

Most of the machinery of an ordinary turbofan is retained; both the compressor and turbines are mounted on the same shaft. The number of blades on each rotor and number of stages in the turbo-machinery are not considered in this study. Since a separate flow turbofan is considered, a separate duct will be present ensuring the bypass of the secondary flow. In Figures 5---9 below, the components shown in the dark blue represents the detonation chamber and the initial converging diverging section seen evidently in figure 7 represents a near constant area diffuser. These figures help in visualization of the integration of detonation chamber and isolator into a turbofan.

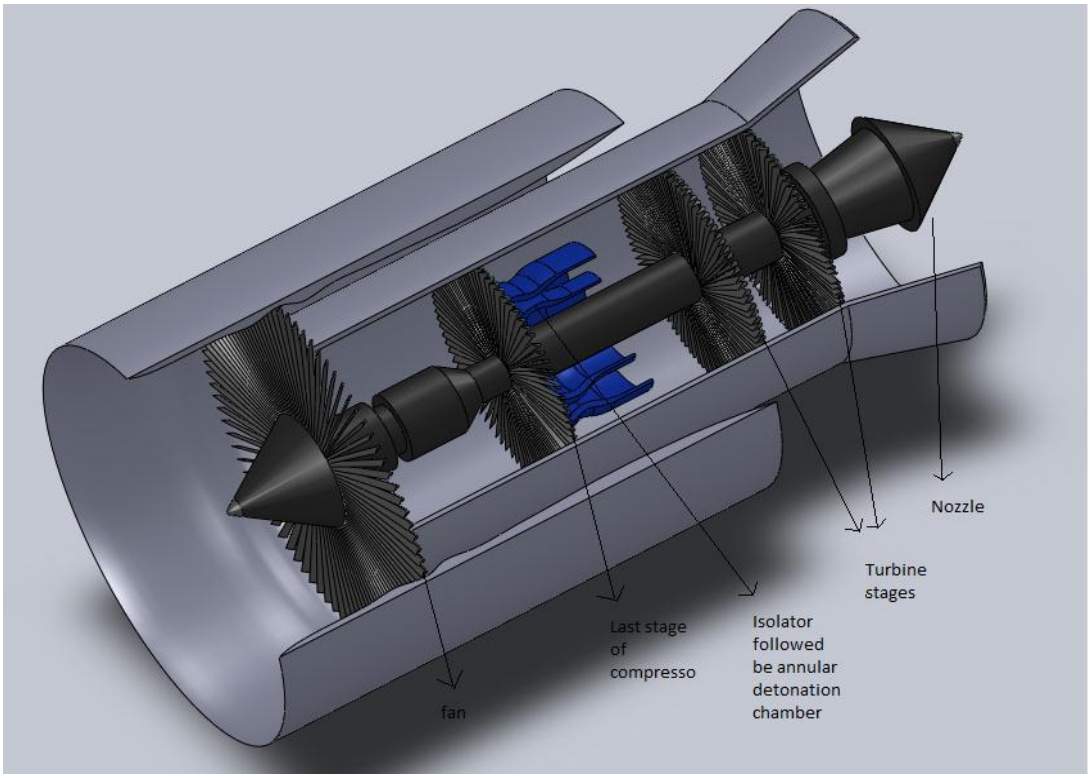

Figure 6 A conceptual sketch of a hybrid turbofan with RDWE.

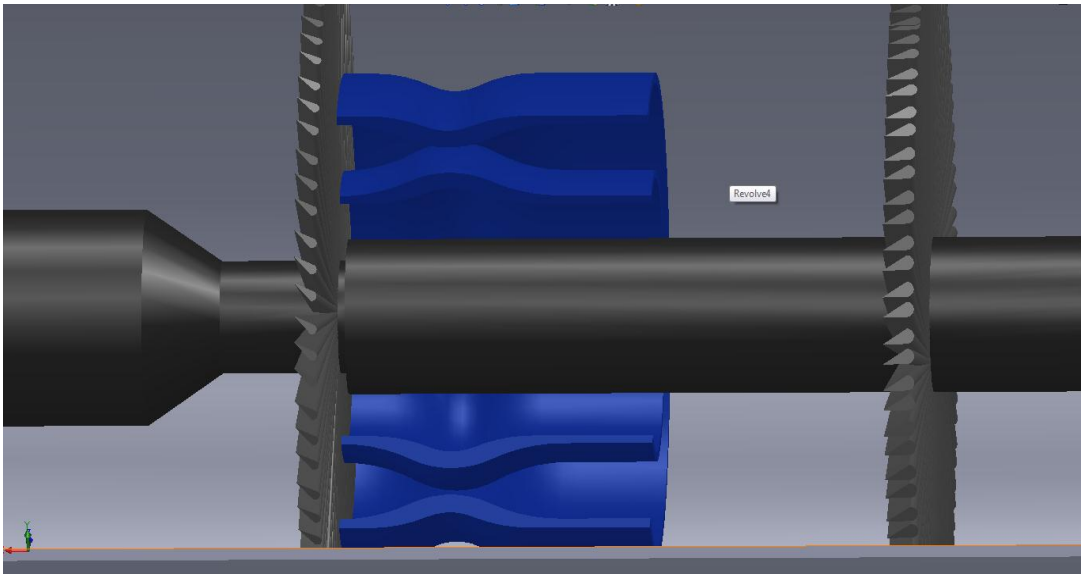

Figure 7 A close-up view of the isolator followed by the detonation chamber.

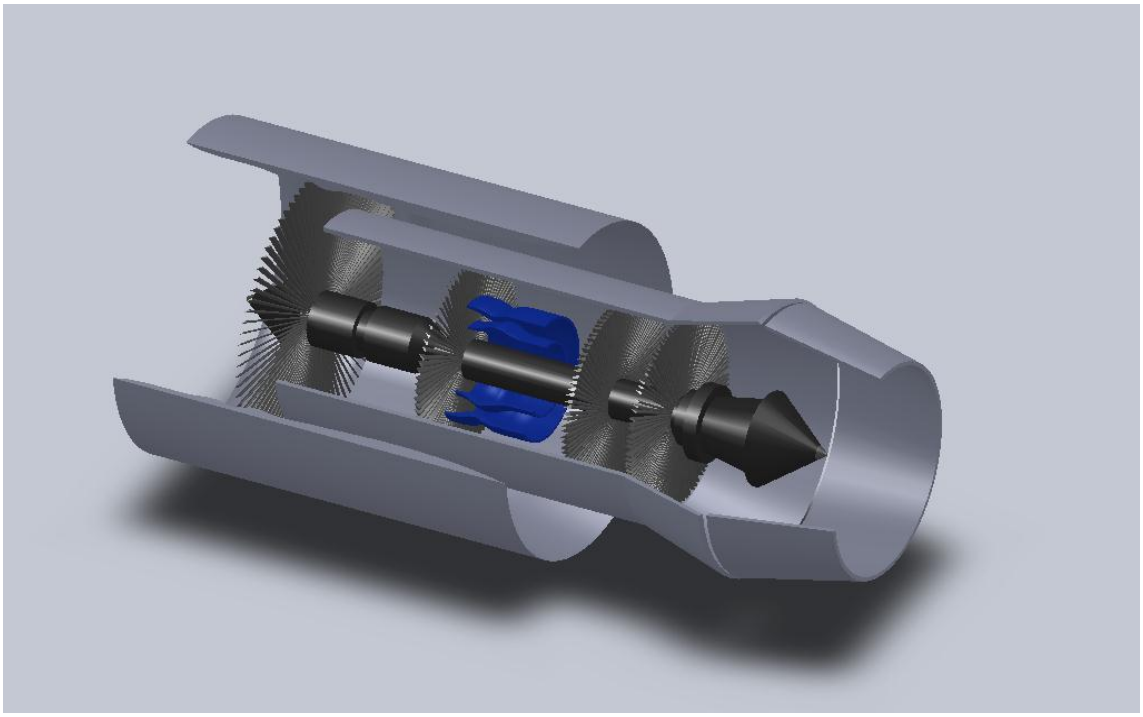

Figure 8 Conceptual sketch of a turbofan integrated with a RDWE.

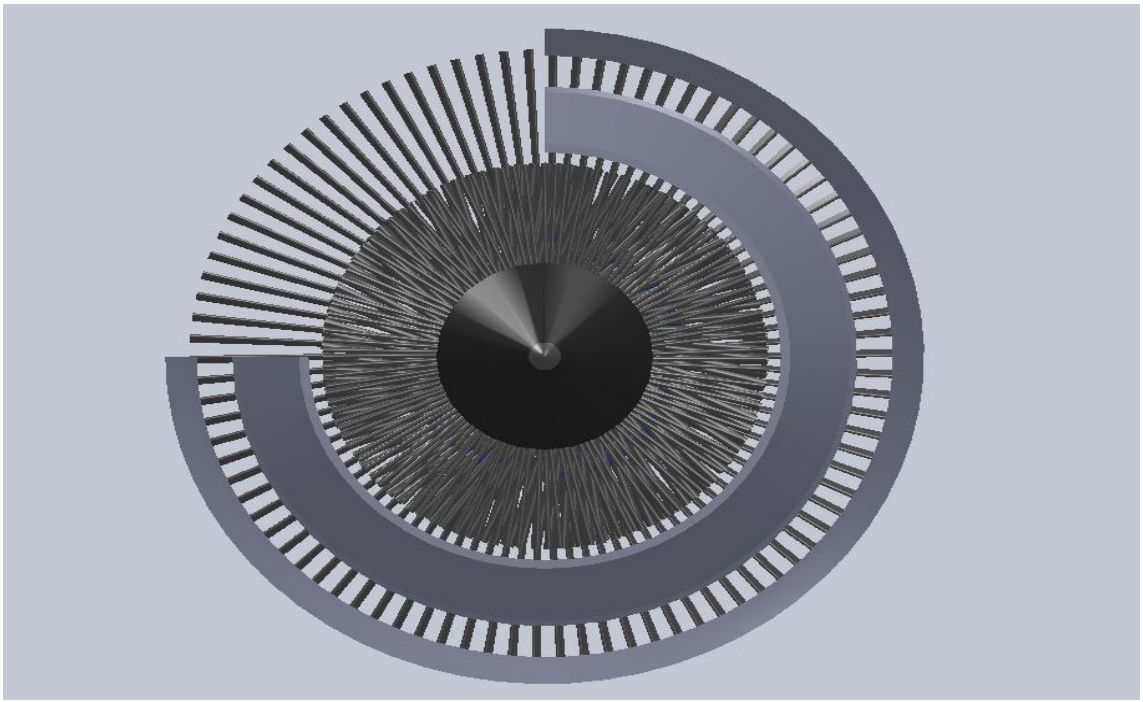

Figure 9 Front view of a turbofan.

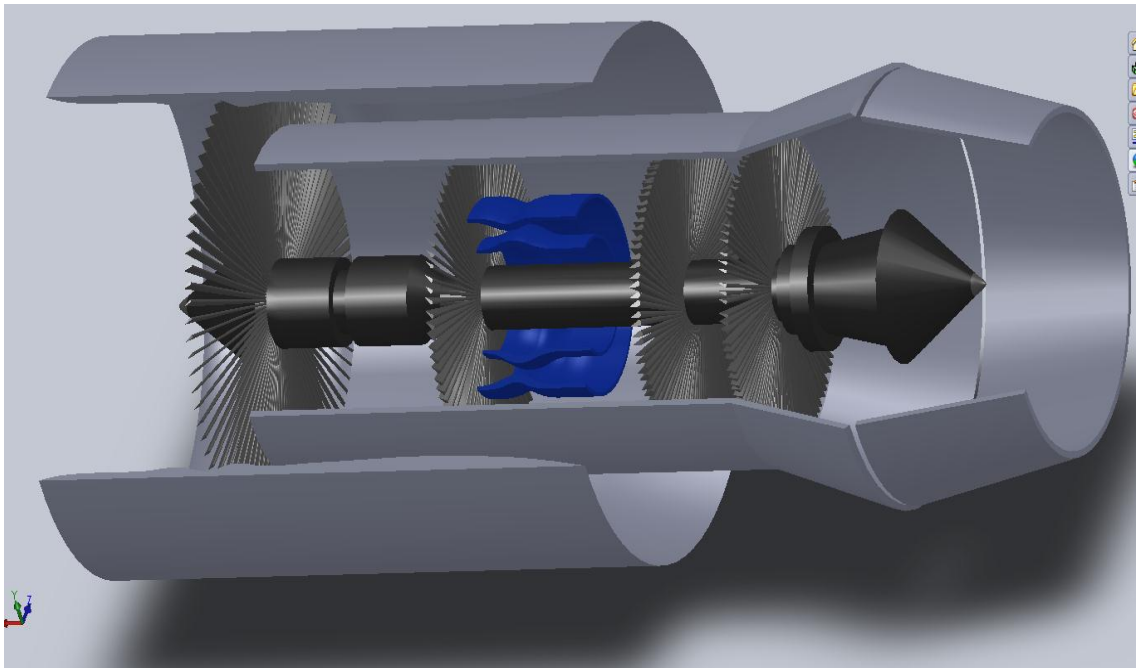

Figure 10 An isometric view of the conceptual hybrid turbofan.

1.4 Method of Analysis

The turbofan with a continuous detonation engine is subjected to parametric analysis using equations as described in chapter 2. Based on this analysis, performance parameters are determined and plotted against each other following a meaningful pattern and compared to the performance plots of a normal turbofan, collectively these plots would give us an understanding of the overall relative engine performance.

1.5 Introduction to Isolator

Since in a detonation process, high pressures are reached in the front section of detonation chamber and a low pressure area exists before the combustor, there is a possibility of a shock wave propagating upstream which might lead to catastrophic failure. Thus, a device called an “isolator” is used, which has a unique capability of suppressing back pressure by providing a “shock wave cushion”. [12] The isolator works on the shock train concept (a series of normal or oblique shock waves) to damp out any shock surge upstream.

A shock train's maximum pressure rise is exactly the same as that of an individual shock wave; it is only longer and gradual, associated with boundary layer separation. For lower supersonic entry Mach numbers usually normal shock wave trains occur and higher entry Mach numbers oblique shock wave trains occur. Due to the effects which are only important when there is a supersonic flight (unstart problem) or an adverse back pressure, which are isolated cases and also due to its complexity, isolator is not considered in the present analysis.

CHAPTER 2

PARAMETRIC ANALYSIS

2.1 Parametric Analysis of a Normal Turbo Fan (NTF)

Parametric cycle analysis desires to determine how the engine performance (specific thrust and fuel consumption) varies with changes in the flight conditions (e.g., Mach number), design limits (e.g., main burner exit temperature), component performance (e.g., turbine efficiency), and design choices (e.g., compressor pressure ratio).[1] The analysis is done through a procedure which follows energy conservation and flow balance. Since a wide range of variables are used as parameters and their variation is studied, it is called parametric analysis, [1] Similar analysis is done with certain modifications at stations 3 & 4 for the HTF (hybrid turbo fan). An open freeware called CEA was used to obtain the detonation parameters. Though these detonation parameters do not affect the performance of the engine directly, the temperature and pressure values at station 4 (combustor exit) do have a direct impact.

The following assumptions are made: [1]

1. Ideal parametric analysis is done where in the losses (aerodynamic, heat, boundary layer, viscous, radiation etc.) are ignored and an ideal gas with constant specific heats is considered.
2. The engine exhaust nozzles expand the gas to the ambient pressure $\left(P_e = P_0\right)$

2.1.1 Parametric Analysis of an Ordinary Turbofan

The following are the assumptions for the cycle analysis of a turbofan with separate exhaust [1] streams:

1. Perfect gas upstream of main burner with constant properties γ_c, R_c, c_{pc} etc.

2. Perfect gas downstream of main burner with constant properties γ_t, R_t, c_{pt} etc.

3. All components are adiabatic i.e. no turbine cooling.The efficiencies of the compressor, fan and the turbine are described through the use of (constant) polytrophic efficiencies e_c, e_f and e_t respectively.

4. The following equations[1] are used for the analysis of a standard turbofan (for a detailed derivation of these equations see [1]):

$$R_c = \frac{(\gamma_c - 1)}{\gamma_c} c_{pc} \tag{12}$$

$$R_t = \frac{(\gamma_c - 1)}{\gamma_t} c_{pc} \tag{13}$$

The local speed of sound given by

$$a_0 = \sqrt{\gamma_c R_c T_0} \tag{14}$$

To calculate velocity, provided Mach number is available:

$$V_0 = a_0 M_0 \tag{15}$$

Static temperature and pressure ratios of the free stream are given by:

$$\tau_r = 1 + (\gamma_c - 1)\frac{M_0{}^2}{2} \tag{16}$$

$$\pi_r = \tau_r{}^{\gamma_c/(\gamma_c - 1)} \tag{17}$$

$$\text{Since } M_0 < 1, \eta_r = 1 \tag{18}$$

By definition τ_λ is the ratio of burner exit enthalpy to ambient enthalpy:

$$\tau_{\lambda} = \frac{c_{pt} T_{t4}}{c_{pc} T_0} \tag{22}$$

The compressor pressure and temperature ratios are related by equation: [1]

$$\tau_c = \pi_c^{\frac{\gamma_c - 1}{\gamma_c e_c}} \tag{23}$$

The compressor efficiency is given by:

$$\eta_c = \frac{\pi_c^{(\gamma_c - 1)/\gamma_c} - 1}{\tau_c - 1} \tag{24}$$

The temperature pressure ratio and the efficiency of the fan is given by equation (25) and (26)

$$\tau_f = \pi_f^{(\gamma_c - 1)/\gamma_c e_f} \tag{25}$$

and

$$\eta_f = \frac{\pi_f^{\gamma_c - 1 / \gamma_c} - 1}{\tau_f - 1} \tag{26}$$

A power balance of the combustor yields

$$f = \frac{\tau_{\lambda} - \tau_r \tau_c}{\frac{\eta_b h_{pr}}{c_{pc} T_0} - \tau_{\lambda}} \tag{27}$$

The power balance between the turbine, compressor, and fan yields

$$\tau_t = 1 - \frac{\tau_r}{\eta_n (1 + f) \tau_{\lambda}} \left[\tau_c - 1 + \alpha (\tau_f - 1) \right] \tag{28}$$

$$\pi_t = \tau_t^{\gamma_t/(\gamma_t - 1)e_t} \tag{29}$$

$$\eta_t = \frac{1 - \tau_t}{1 - \tau_t^{1/e_t}} \tag{30}$$

$$\frac{P_{t9}}{P_9} = \frac{P_0}{P_9}\pi_r\pi_d\pi_c\pi_b\pi_t\pi_n \tag{31}$$

The exit Mach number is

$$M_9 = \frac{2}{\gamma_t - 1}\left(\frac{P_{t9}}{P_9}\right)^{\sqrt{\gamma_t - 1/\gamma_t - 1}} \tag{32}$$

$$\frac{T_9}{T_0} = \frac{\tau_\lambda\tau_t}{\left(P_{t9}/P_9\right)^{\frac{\gamma_t - 1}{\gamma_t}}}\frac{c_{pc}}{c_{pt}} \tag{33}$$

Expressing velocity ratios in terms of Mach numbers, temperatures, and gas properties of states 0 and 9:

$$\frac{V_9}{a_0} = M_9\sqrt{\frac{\gamma_t R_t T_9}{\gamma_c R_c T_0}} \tag{34}$$

The ratio of total pressure of the fan to static pressure is given by:

$$\frac{P_{t19}}{P_{19}} = \frac{P_0}{P_{19}}\pi_r\pi_c\pi_f\pi_{fn_d} \tag{35}$$

$$M_{19} = \sqrt{\frac{2}{\gamma_c - 1}\left[\left(\frac{P_{t19}}{P_{19}}\right)^{(\gamma_c - 1)/\gamma_c} - 1\right]} \tag{36}$$

$$\frac{T_{19}}{T_0} = \frac{\tau_r \tau_f}{\left(P_{t19}/P_{19}\right)^{(\gamma_c - 1)/\gamma_c}} \tag{37}$$

$$\frac{V_{19}}{a_0} = M_{19}\sqrt{\frac{T_{19}}{T_0}} \tag{38}$$

Combining the thrust equation for the fan stream and the engine core stream, we obtain

$$\frac{F}{m_0} = \frac{1}{1+\alpha}\frac{a_0}{g_c}\left[(1+f)\frac{V_9}{a_0} - M_0 + (1+f)\frac{R_t T_9/T_0}{R_c V_9/a_0}\frac{1-P_0/P_{19}}{\gamma_c}\right] + \left[\frac{\alpha}{1+\alpha}\cdot\frac{a_0}{g_c}\left[\frac{V_{19}}{a_0} - M_0 + \frac{T_{19}/T_0}{V_{19}/a_0}\frac{1-P_0/P_{19}}{\gamma_c}\right]\right] \tag{39}$$

The thrust specific fuel consumption S is

$$S = \frac{f}{(1+\alpha)F/m_0} \tag{40}$$

The propulsive and thermal efficiencies are given by

$$\eta_P = \frac{2M_0\left[(1+\alpha)V_9/a_0 + (\alpha V_{19}/a_0) - (1+\alpha)M_0\right]}{(1+f)(V_9/a_0)^2 + \alpha(V_9/a_0)^2 - (1+\alpha)M_0^2} \tag{41}$$

$$\eta_t = \frac{a_0^2(1+f)(V_9/a_0)^2 + \alpha(V_{19}/a_0) - (1+\alpha)M_0^2}{2fh_{pr}} \tag{42}$$

The overall efficiency:

$$\eta_0 = \eta_p \eta_T \tag{43}$$

2.2 Parametric Analysis of Hybrid Turbo Fan (HTF)

In a HTF, due to the addition of a detonation chamber corresponding modifications needs to be done in the analysis procedure of a standard turbofan. Section 2.2.1 and 2.2.2 will give more details on the modifications adapted.

2.2.1 Temperature at station 4

Section 2.1 gives us the performance of a standard turbofan without any kind of integration with new technology. HTF is integrated with a detonation chamber, therefore we need to modify the above set of equations so that it takes into account the effect of detonation occurring inside and reflect that in the performance. To do such an analysis of HTF, first we need to calculate the detonation parameters (temperature, pressure, density, etc. changes) inside the detonation chamber which are sensitive to the type of fuel, initial pressure, initial temperature, and fuel–air ratio. Thus for the sake of simplicity we shall keep most of these parameters constant and use CEA to calculate the detonation parameters inside the detonation chamber. As we do so, we face another problem: CEA gives the values of temperature, pressure, specific heat ratio, velocity etc. directly behind the detonation wave as output, when the values of the certain variables ahead of (combustor entry/station 3) the detonation wave are given as an input. Thus, the values of temperature and pressure are those of points immediately behind the detonation front and not at station 4 of the turbofan.

This problem is addressed by averaging the temperature and pressure over the entire span of the wave propagation. To do this, pressures and temperatures are determined at each point defined by a variable r, which represents the locus of the TDW path and is essentially the circumference of the chamber, and averaging it over the entire range. [7]

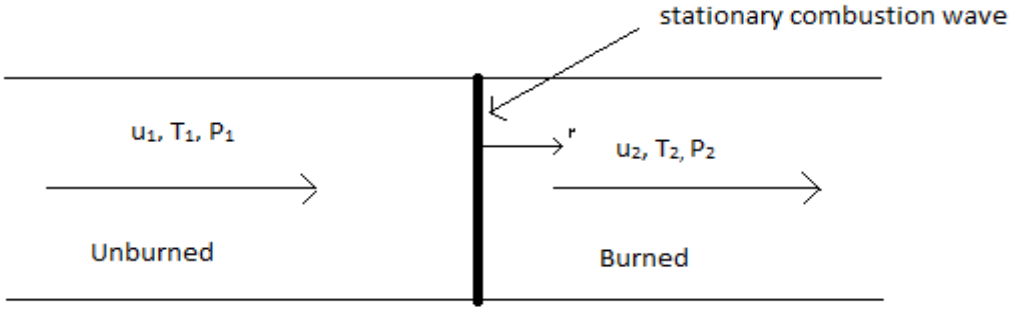

Figure 11 Rolled out view of the annular chamber denoting the parametric variable 'r'.

The pressure and temperature at each point r are given by [7]

$$P_r = P_{cj}\left(\frac{1}{\gamma_{cj}} + \frac{\gamma_{cj}-1}{\gamma_{cj}}\frac{C-r}{C}\right)^{\frac{2\gamma_{cj}}{\gamma_{cj}-1}}\left[\frac{h}{\left(h+r\sin\left(\upsilon_{\max}\right)\right)^{\gamma_{cj}}}\right]^{\gamma_{cj}} \tag{44}$$

$$T_r = T_{cj}\left(\frac{P_r}{P_{cj}}\right)^{\frac{\gamma_{cj}-1}{\gamma_{cj}}} \tag{45}$$

The average of the temperature will give us the exit temperature at station 4:

$$T_{avg} = T_4 = \frac{\sum T_r}{N_r} \tag{46}$$

Where N_r is the total number of points at which the temperature was considered.

Similarly the pressure:

$$P_{avg} = P_4 = \frac{\sum P_r}{N_r} \tag{47}$$

When P_r is plotted against r we obtain Figure 12.

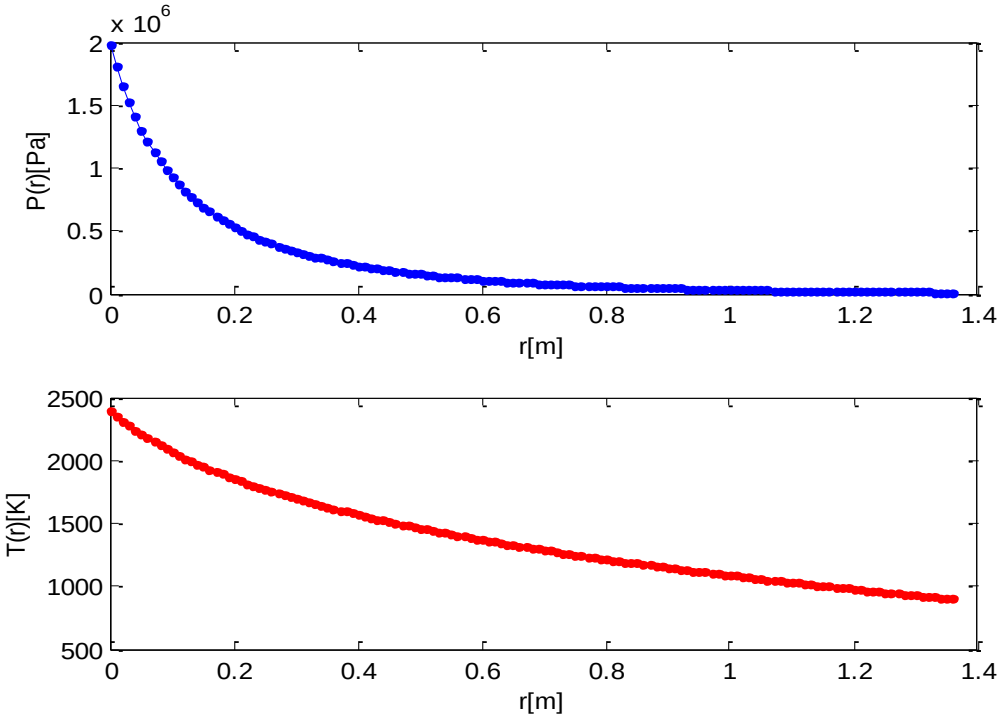

Figure 12 A typical distributions of pressure and temperature as a function of r .

Figure 12 is a graphical representation of the temperature and pressure distribution at each point r , obtained after solving equation (44) and (45) at each r . The equilibrium CJ point parameters are obtained via CEA. See appendix B, code for more details.

The values of T_4 and P_4 can used to find the total temperatures at station 4 required in the analysis of HTF:

$$T_{t4} = T_4\left(1+\left(\frac{\gamma_2 - 1}{2}\right)M_4^2\right) \tag{48}$$

$$P_{t4} = P_4\left(1+\left(\frac{\gamma_2 -1}{2}\right)M_4^2\right)^{\frac{\gamma_2}{\gamma_2 -1}} \tag{49}$$

Using Equations (48) and (49) we can evaluate:

$$\tau_b = \frac{T_{t4}}{T_{t3}} \tag{50}$$

$$\pi_b = \frac{P_{t4}}{P_{t3}} \tag{51}$$

2.2.2 Modifications required: Mach number at station 4.

Equation (48) and (49) still need the exit Mach number of the combustor, M_4 which can be determined by specifying values for certain geometric properties for the chosen model.

For fuel–oxidizer choice of hydrogen and air we have: [3]

$$a = 0.0156 \text{ m} \tag{52}$$

The parameter a being the width of the self-excited cell.This parameter is easily determined by known established methods and is already available for a wide range of mixtures. For Hydrogen-air combination, (52) is determined using table 2.

The distance between neighboring detonation waves:

$$l = \frac{\pi d_c}{n} \tag{56}$$

The following equation relates the total stagnation enthalpy of the mixture to the detonation wave velocity:

$$\left(2J_0 + D^2\right)/q_2^2 = (\gamma+1)/(\gamma-1) \tag{57}$$

Where D is the velocity of the detonation wave itself and is obtained directly from CEA. The total stagnation enthalpy of the mixture entering the detonation chamber 'J_0' is then determined using:[3]

$$J_0 = \frac{q_2^2 \frac{\gamma+1}{\gamma-1} - D^2}{2} \tag{58}$$

The above equation is an alternative form of the Hugoniot equation expressed in terms of total enthalpy. Further the velocity V is given by the equation [3]:

$$V = \sqrt{\frac{2 \cdot (\gamma-1) J_0}{(\gamma+1)}} \tag{59}$$

To incorporate a part of mass flux that comes into the detonation wave under study from the previous detonation wave which has just preceded, a factor called k is introduced; for our current study. We will assume a value,

$$k = 0.15 \tag{60}$$

The values of $q_2, a_2, \gamma_1, \gamma_2, c_{p,} T_{2,}$ are obtained from CEA software which determines Chapman-Jouguet wave parameters.

Total mixture flow rate for a single wave, specific mixture flow rate, density, pressure and Mach number are given by following equations:

$$G_1 = (1-k) h \rho_2 q_2 \Delta = h_1 \Delta \rho_2 q_2 \tag{61}$$

$$g = \frac{G_1}{\Delta \cdot l} \quad \frac{\text{Kg}}{\text{ms}^2} \tag{62}$$

$$\rho = \frac{g}{V} \quad \frac{\text{Kg}}{\text{m}^3} \tag{63}$$

$$P = \frac{gV}{\gamma_2} \tag{64}$$

$$M_4 = \frac{V}{a_2} \tag{65}$$

So now we have all the inputs required for the parametric analysis of the HTF, with equations similar to those used for the analysis of a standard turbofan (energy and flow balance equations). Once the new values of τ_b and π_b are substituted for the previous ones, various performance parameters can thus be determined and compared with that of a NTF.

2.2.3 Flow Chart of the Complete Parametric Analysis of a HTF

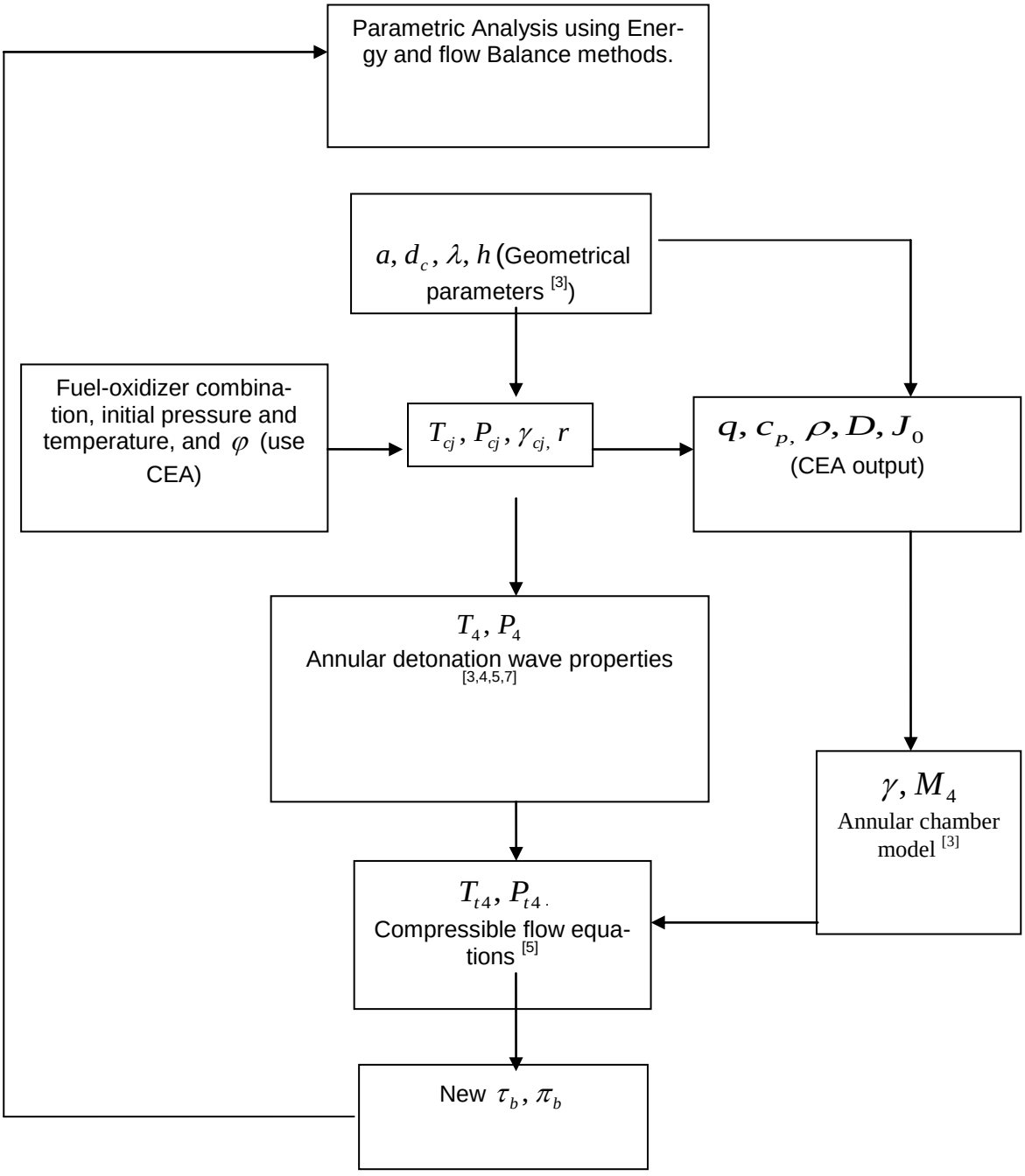

Figure 13 Flow chart of the parametric analysis .

2.3 CEA [11] (Chemical Equilibrium with Applications)

The NASA program CEA calculates chemical equilibrium compositions and properties of a wide range of fuel-oxidizer mixtures. Applications include assigned thermodynamic states, theoretical rocket performance, Chapman-Jouguet detonations, and shock-tube parameters for incident and reflected shocks. CEA represents the latest in a number of computer programs that have been developed at the NASA Lewis (now Glenn) Research Center during the last 45 years. [11] Over 2000 species are contained in the thermodynamic database. The program is written in ANSI standard FORTRAN by Bonnie J. McBride and Sanford Gordon. [11]

Inputs required for Chapman-Jouguet detonation process:

- Chemical equivalence ratio: (φ): this ratio indicates the ratio of fuel to oxidizer. A ratio of one ensures maximum combustion.
- Fuel-oxidizer choice: Out of the 2000-odd chemical species available an appropriate detonation mixture needs to be selected.
- Initial temperature and pressure

An example of a CEA output is partially shown in Tables 3-6 below:

Detonation properties of an ideal reacting gas

Case = Air-hydrogen

Table 3 CEA output.

REACTANT		WT FRACTION	Energy (KJ/KG-Mole)	T (K)
Fuel	H2	1.0000000	53.359	300.000
Oxidant	Air	1.0000000	-71.689	300.000

O/F= 1.00000 %FUEL= 50.000000 R, EQ.RATIO=34.245598 PHI, EQ.RATIO=34.296226

Table 4 Values of variables ahead of the TDW (unburned gas).

P_1, BAR	1.0132
T_1, K	300.00
H_1, KJ/KG	-1.65
M_1, (1/n)	21.008
$GAMMA_1$	1.4046
SONIC VEL_1,M/SEC	407.9

Table 5 Values of variables behind the TDW (burned gas).

P, BAR	15.696
T, K	2934.85
RHO, KG/CU M	1.5394 0
H, KJ/KG	1335.47
U, KJ/KG	315.89
G, KJ/KG	-29842.8
S, KJ/(KG)(K)	10.5910
M, (1/n)	24.007
Cp, KJ/(KG)(K)	-1.00957
GAMMAs	1.1636
SON VEL,M/SEC	1089.2

Table 6 Detonation parameters.

P/P1	15.491
T/T1	9.813
M/M1	1.1427
RHO/RHO1	1.8039
DET MACH NUMBER	4.8169
DET VEL, M/SEC	1964.9

Table 3 indicates which combination of fuel-oxidizer mixture are being used, their temperature, heat of formation, and relative weight fractions. Table 4 contains more information about the explosive mixture which is directly ahead of the TDW (unburned gas) which includes pressure, temperature, ratio of specific heats, local speed of sound, specific heat of the mixture, and the molecular weight of the mixture. Apart from these, table 5 and table 6 list the values of several other variables/parameters of detonation of which density, molar standard state enthalpy, local speed of sound behind the TDW, ratio of specific heats, specific heat, detonation Mach number, and detonation velocity are the ones we use in our calculation.

In this chapter we saw how the parametric analysis of a standard turbofan is modified to fit a detonation-type turbofan. In chapter 3 we will see the actual methods for calculations, assumptions made, code descriptions and results obtained.

As the flight condition changes, input conditions to the burner change as well. To account for those changes, input temperature and pressure to the burner are calculated using the following compressible flow equations.

$$P_3 = \frac{\pi_c \pi_f P_0 \left(1 + \frac{\gamma - 1}{2} M_0^2\right)^{\frac{\gamma}{\gamma - 1}}}{\left(1 + \frac{\gamma - 1}{2} M_3^2\right)^{\frac{\gamma}{\gamma - 1}}} \tag{66}$$

$$T_3 = \frac{\tau_c \tau_f T_0 \left(1 + \frac{\gamma - 1}{2} M_0^2\right)}{\left(1 + \frac{\gamma - 1}{2} M_3^2\right)} \tag{67}$$

The data obtained from the equations (66) and (67) are given in the appendix C

CHAPTER 3

CALCULATIONS AND RESULTS

3.1 Method of calculation

Calculations for a HTF is done by coupling the data from CEA, Table 3--6 to the Matlab code, and executing the code given in appendix A. The output is a huge array of numbers, which were tabulated and plotted. Partial validation of these codes was done by comparing the results with a standard text book problem and its solution; they were in excellent agreement.

The equations were programmed in Matlab. Appendix A is the Matlab code for the HTF and appendix B is the Matlab code for the standard turbofan. The code in appendix A has several bits to it; it begins with vectorizing the input variables. Following which there are bits of code which calculate the exit Mach number, exit temperature and pressure at station 4, in turn determining the new τ_b and π_b. Then the next part of the code substitutes the new values of τ_b and π_b for the old ones and the parametric analysis procedure is followed as in chapter 2 to find the performance parameters. See appendix A for more details.

The calculations presented here include certain assumptions as listed below:

1. U.S standard pressure and atmosphere values are used.
2. For simplicity M_3= 0.5.
3. Value of $k = 0.15$, equation (60).
4. Subsonic flight.

A detailed procedure of obtaining the below plots is as follows:

Table 7 Base values of parameters in a NTF

M_0=0.7	T_0=390^o R
γ_c=1.4	C_{pc}=0.240 Btu/lbm.^{o}R
$\gamma_{t=}$1.33	C_{pt}=0.276 Btu/lbm.^{o}R
h_{pr}=18400 Btu/lbm	π_{dmax}=0.99
π_b=0.96	π_n=0.99
π_{fn}=0.99	e_c=0.90
e_f=0.89	et=0.89
η_b=0.99	η_n=0.99
P_0/P_9=0.99	P_0/P_{19}=0.99
T_{t4}=3000^{o}R	π_c=3
π_f=1.2	α=0.5

Table 7 shows all the parameters and their base values used in the calculation of the performance parameters; polytrophic efficiencies η_b, η_n are kept constant to simplify the calculations. Burnt gas (core flow) and the secondary flow are assumed to expand to ambient pressure thus P_0/P_9, and P_0/P_{19} are very close to unity. The only parameters which will be varied are $M_{0,}\, \pi_c, \pi_f$, and α. Also, h_{pr} is a parameter which is a constant for a specific fuel. The rest of the parameters are assumed constant throughout the calculations.

For a HTF π_b and T_{t4} are calculated from the values obtained from CEA and the method described in chapter 2, then substituted for the old values and the performance analysis is done using the code in Appendix A.

In figures 13—22 certain performance parameters are plotted and compared, definitions of these parameters are given below: [1]

1. Specific thrust ($F / \dot{m}$): It is defined as the ratio of net thrust to the rate of total airflow intake.

2. Thrust specific fuel consumption (S): It is the rate of fuel used by the propulsion system per unit rate of thrust produced.

3. Propulsive efficiency (η_p): It is a degree of how effectively the engine power is used to power the aircraft. It is also the ratio of aircraft power (thrust times velocity) to the power output of the engine.

4. Thermal efficiency (η_T): It is the net rate of organized energy (shaft power or kinetic energy) out of the engine to the rate of thermal energy available from the fuel-air mixture.

5. Overall efficiency (η_0): It is the ratio of aircraft power to the ratio of thermal energy released. It equals the product of propulsive efficiency and thermal efficiency

For figure 13—17 the following flight conditions and design inputs were used:

$M_0 = 0.7, T_0 = 390\ ^o\text{R},\ T_{t4} = 3000\ ^o\text{R}$ (only for a standard turbofan), and $\pi_f = 1.2$.

For figure 18—22 the following flight conditions were used:

$\pi_c = 1.5, T_0 = 390\ ^o\text{R},\ T_{t4} = 3000\ ^o\text{R}$ (only for a standard turbofan), and $\pi_f = 1.2$.

3.2 Comparison plots

The following graphs are obtained.

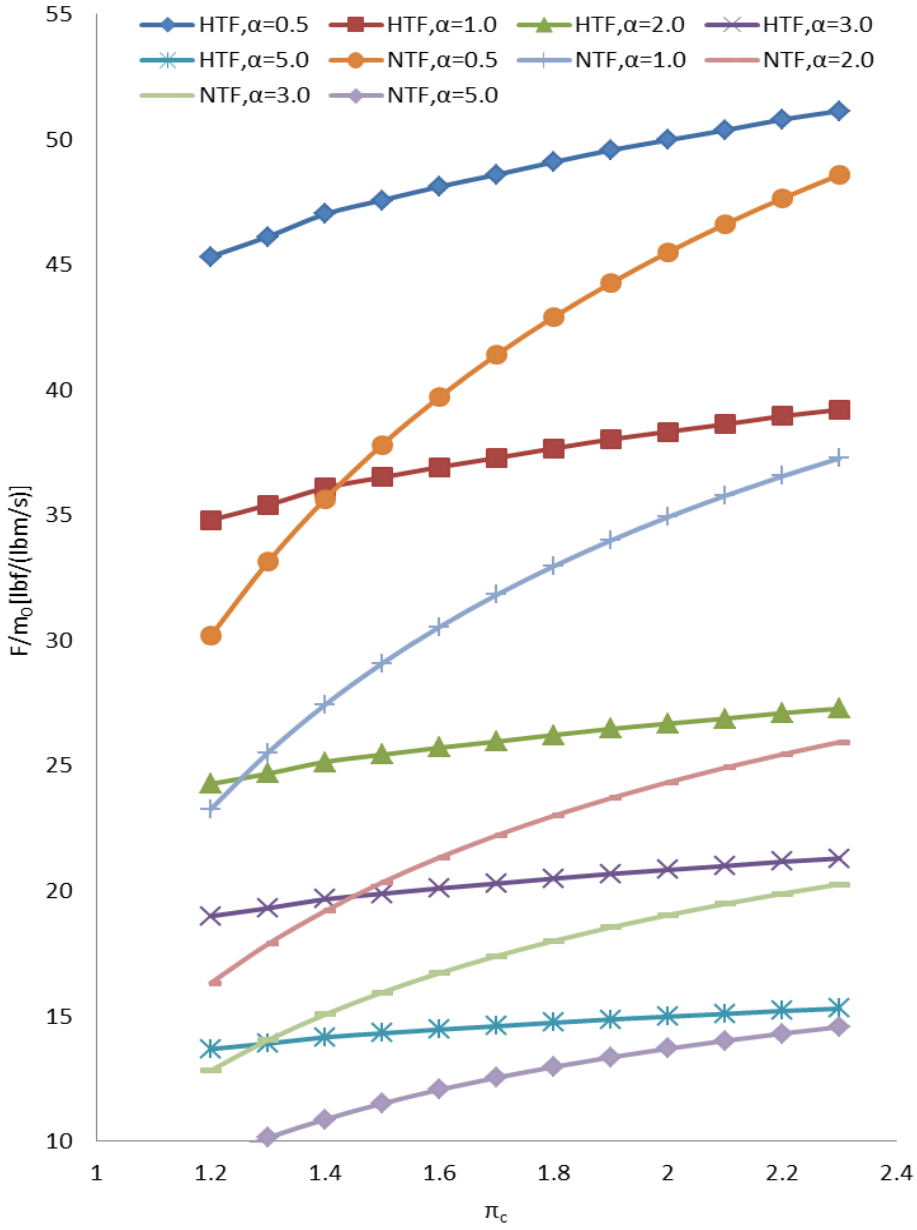

Figure 14 Performances of NTF and HTF versus π_c, for π_f=1.2 and M_0=0.7.

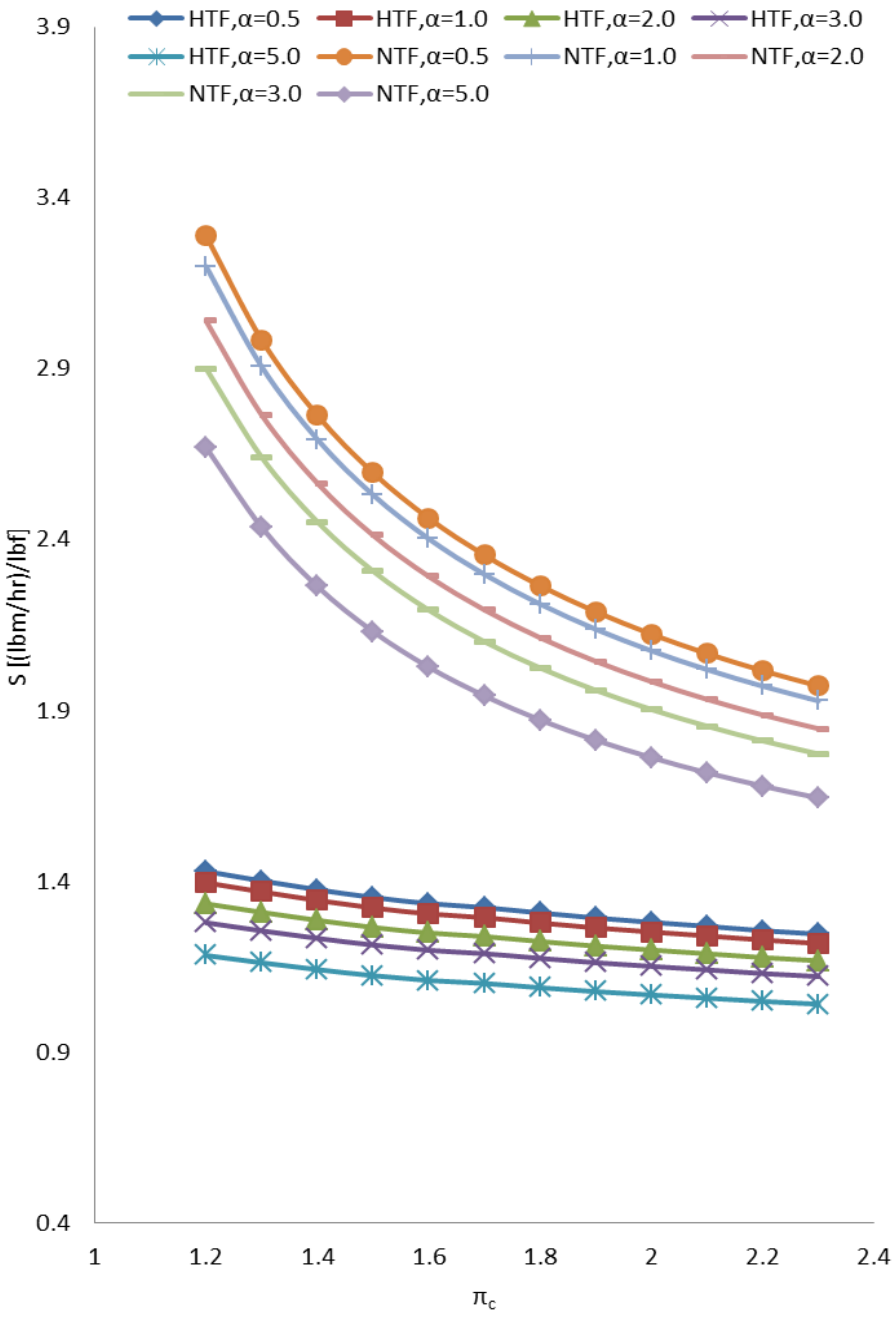

Figure 15 Performances of NTF and HTF versus π_c, for π_f=1.2 and M_0=0.7.

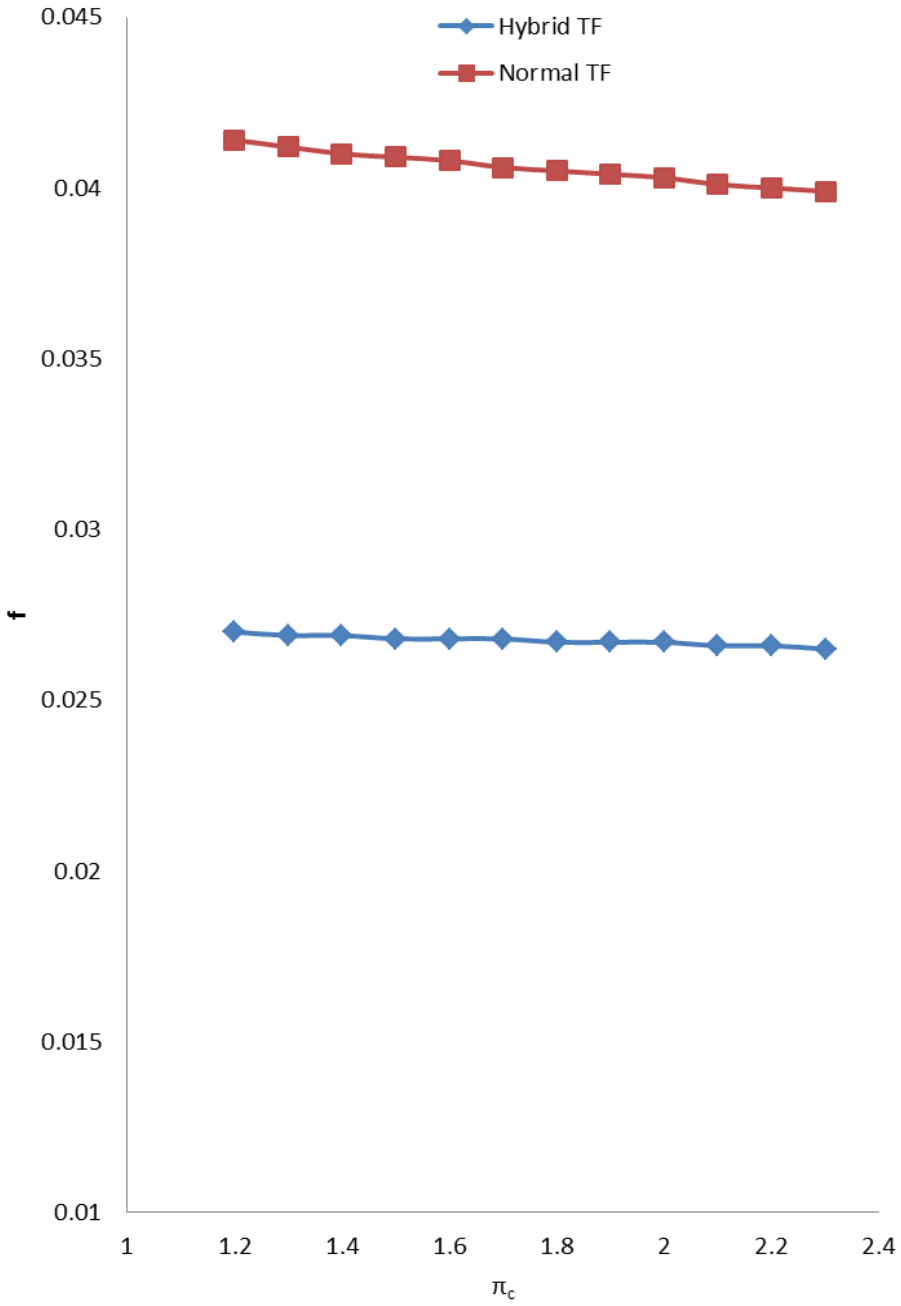

Figure 16 Comparison of performances of NTF and HTF versus π_c, for π_f=1.2 and M_0=0.7

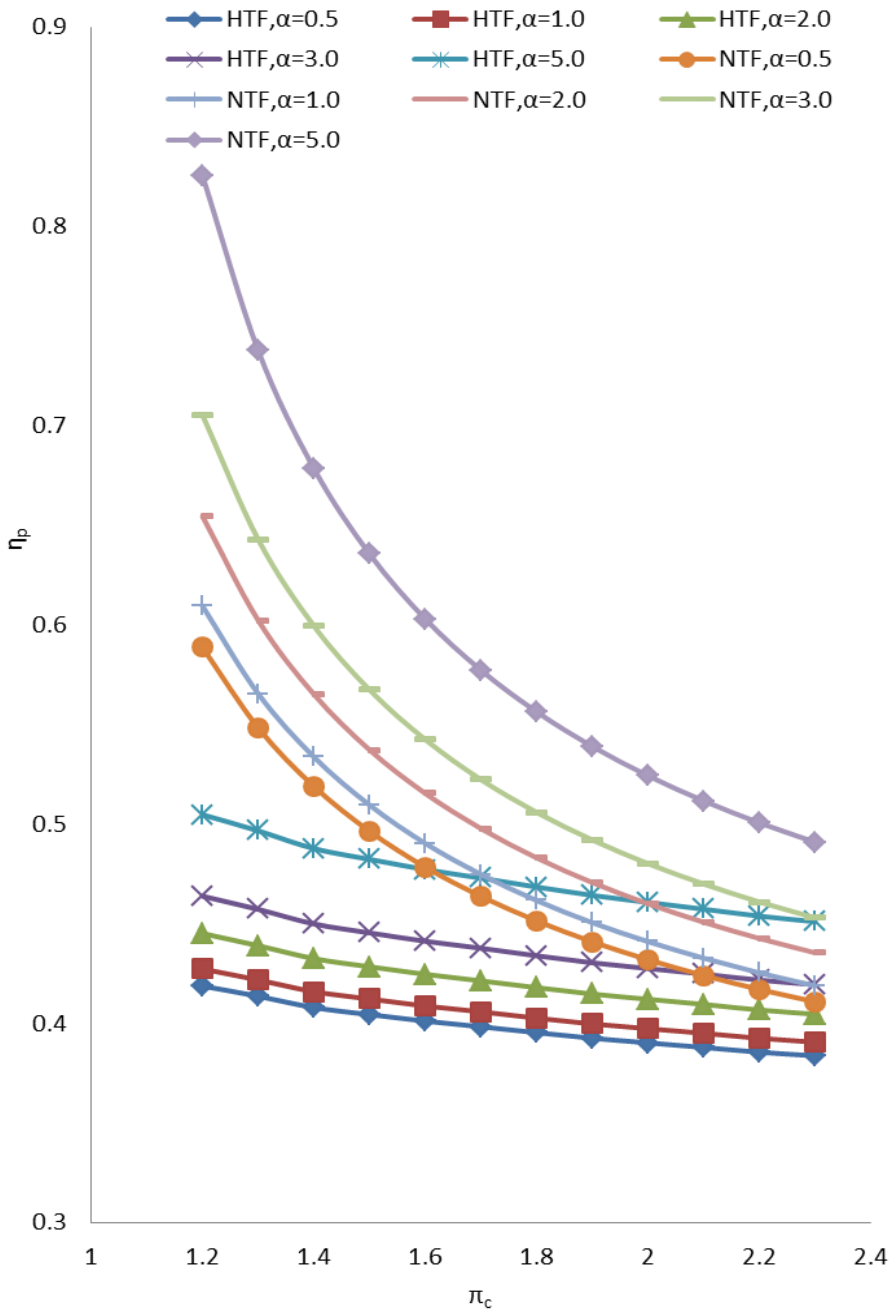

Figure 17 Comparison of performances of NTF and HTF versus π_c, for π_f=1.2 and M_0=0.7

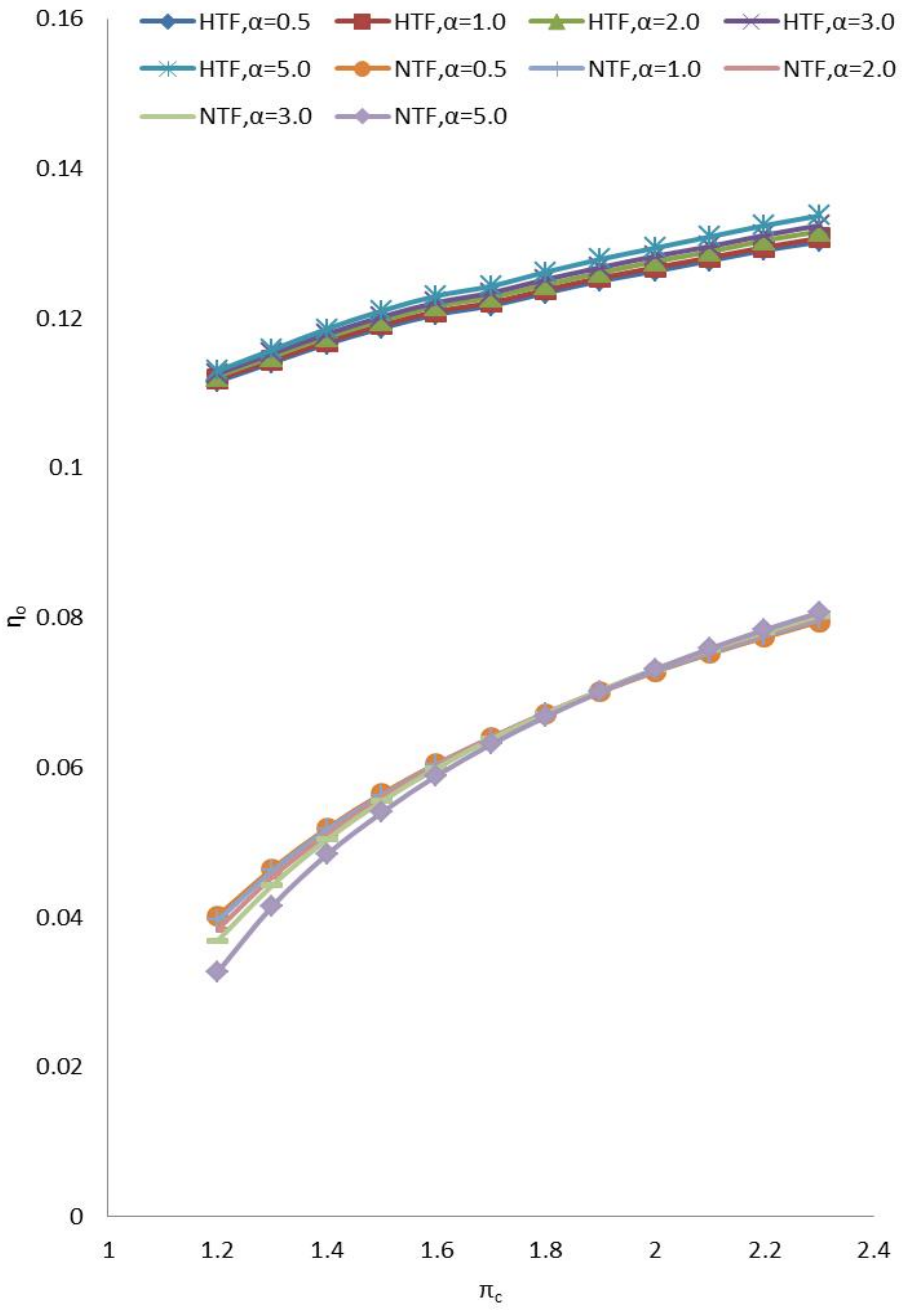

Figure 18 Comparison of performances of NTF and HTF versus π_c, for π_f=1.2 and M_0=0.7

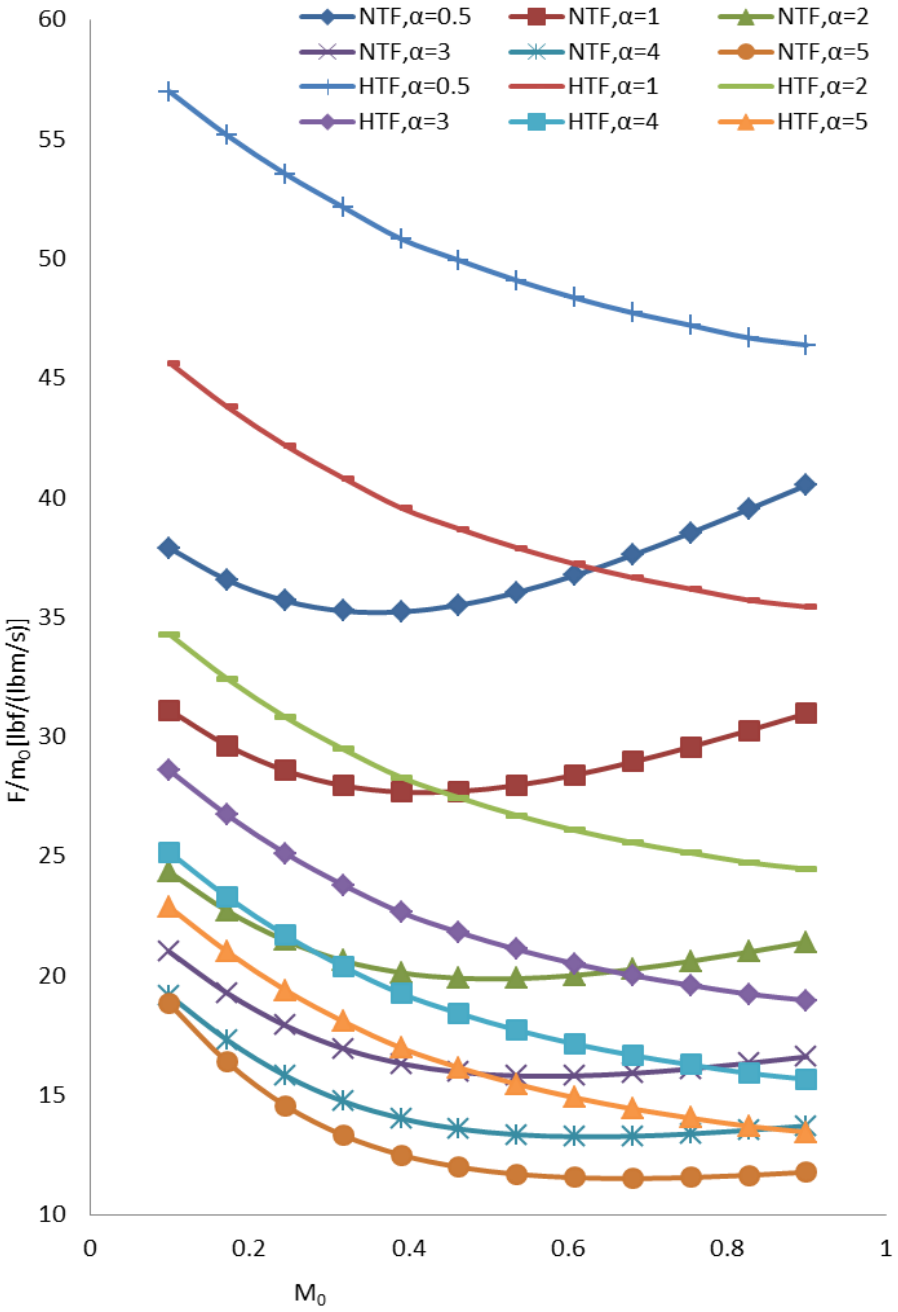

Figure 19 Comparison of performances of NTF and HTF versus M_0, for π_f=1.2 and π_c=1.5

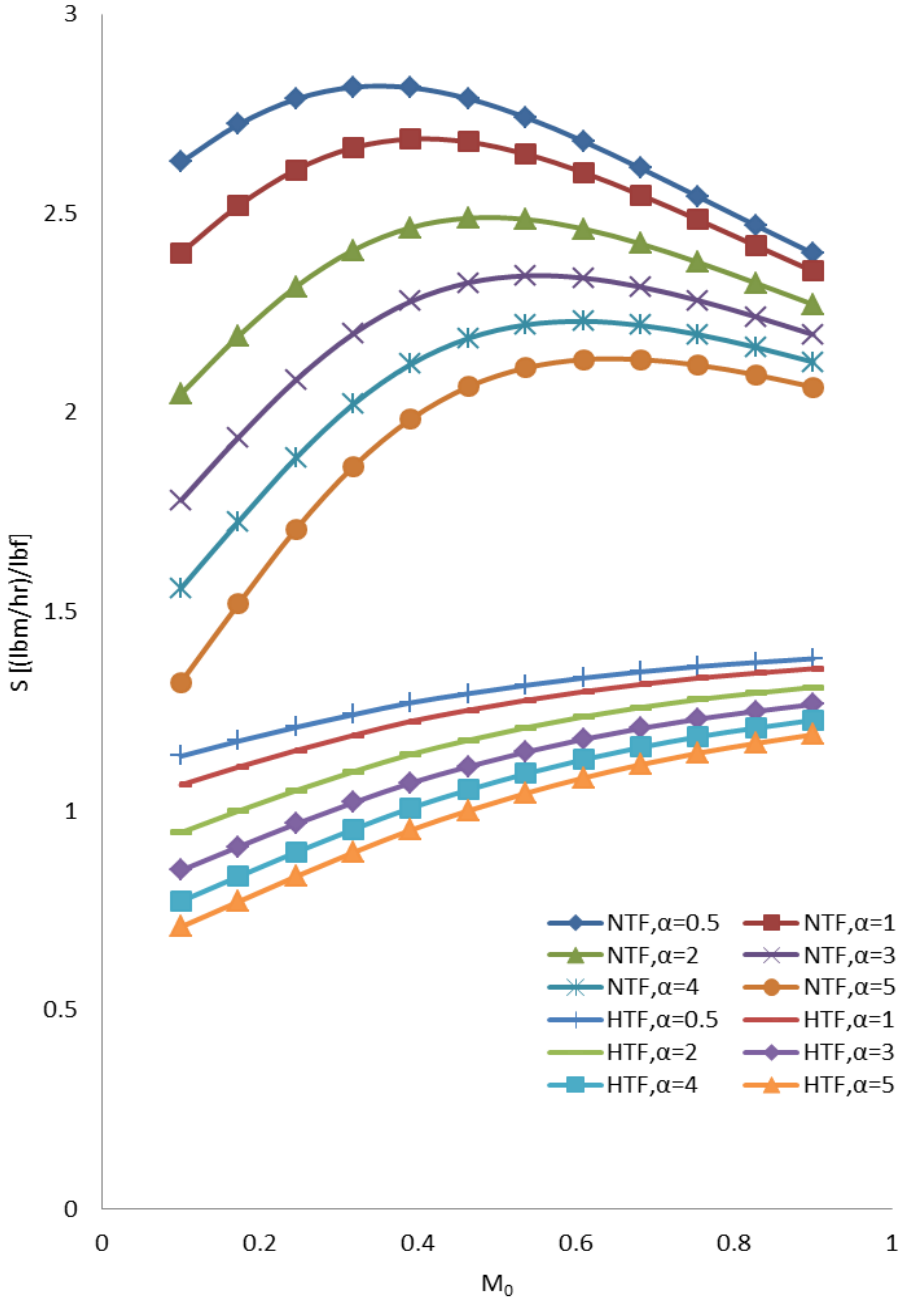

Figure 20 Comparison of performances of NTF and HTF versus M_0, for $\pi_f = 1.2$ and $\pi_c = 1.5$

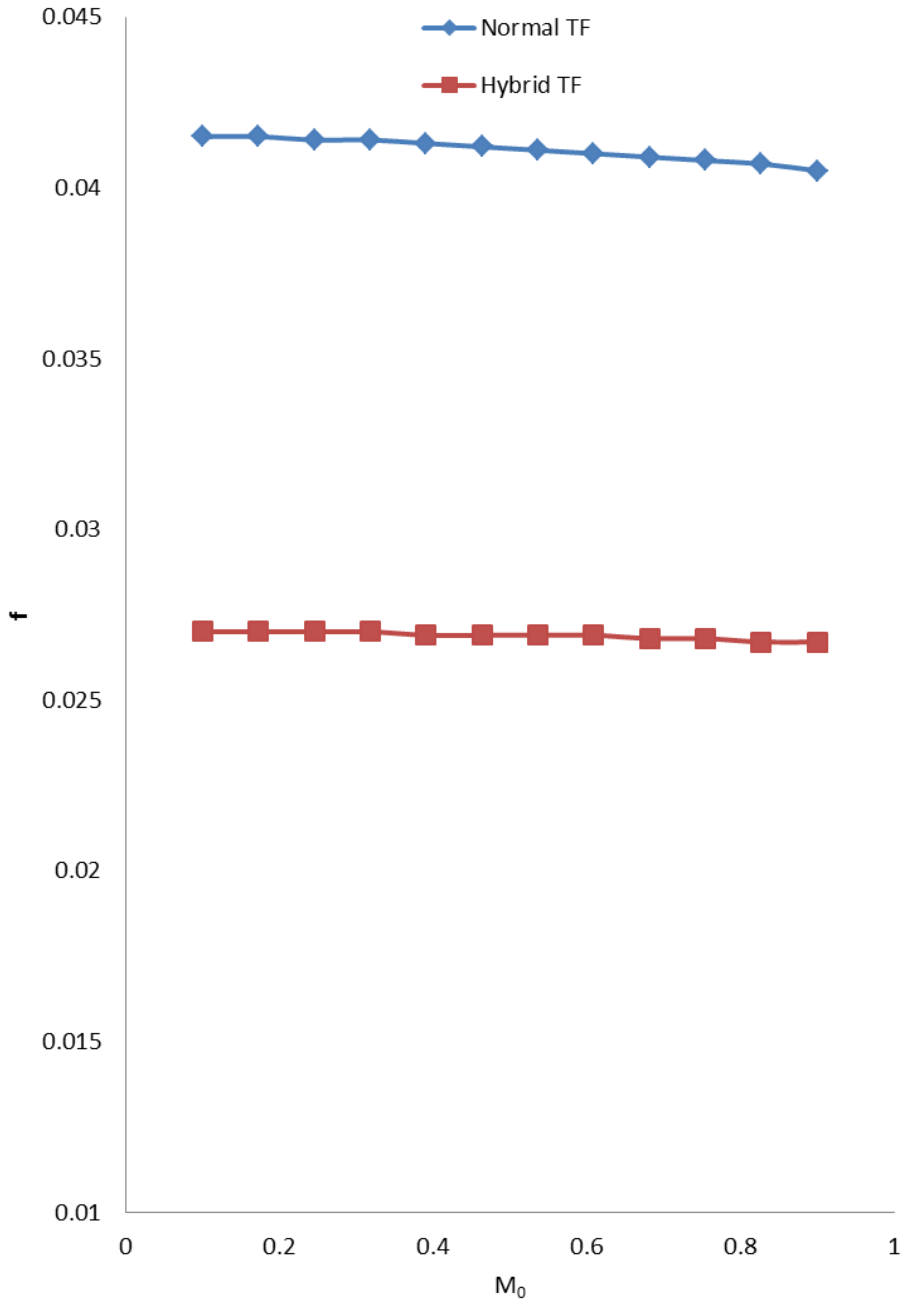

Figure 21 Comparison of performances of NTF and HTF versus M_0, for π_f=1.2 and π_c=1.5

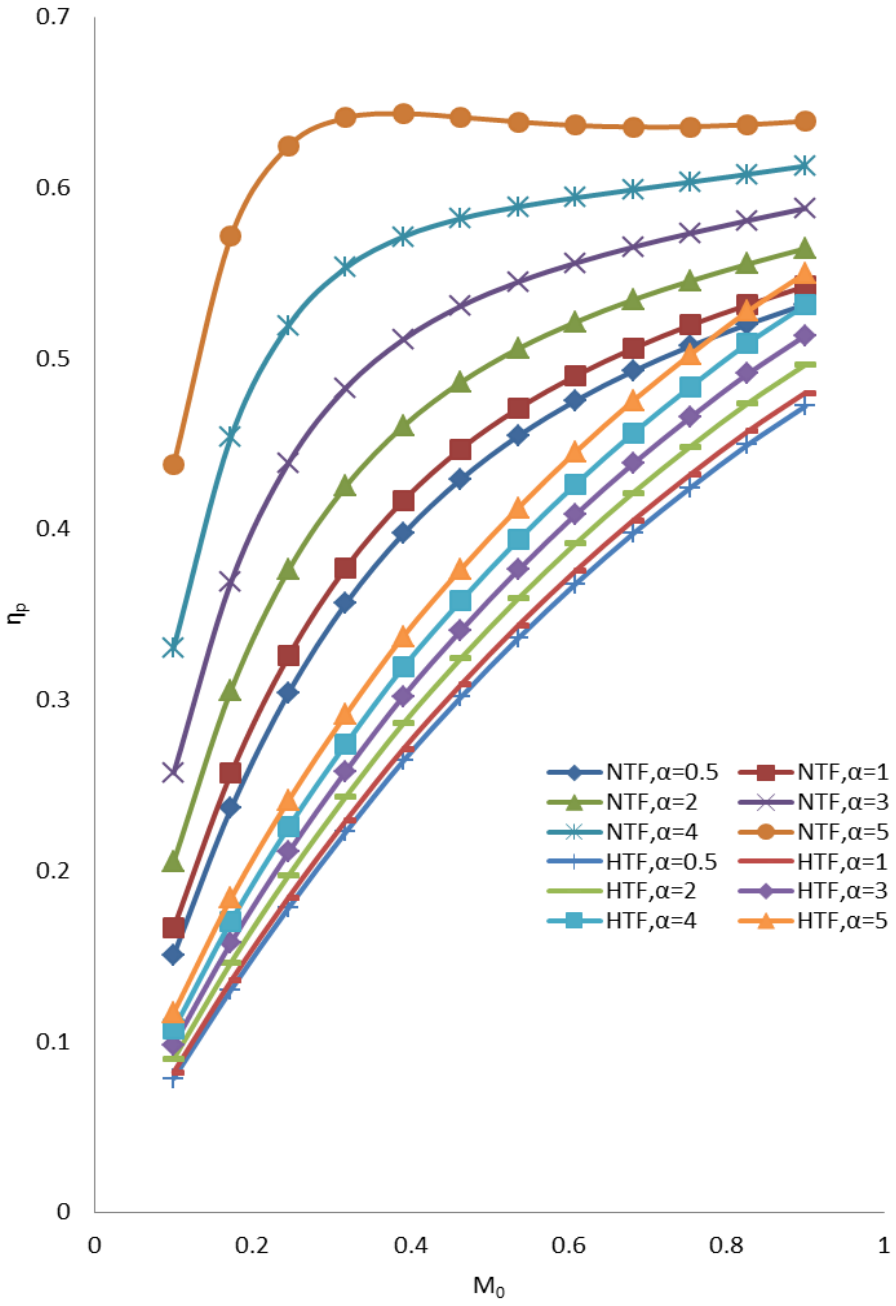

Figure 22 Comparison of performances of NTF and HTF versus M_0, for π_f=1.2 and π_c=1.5

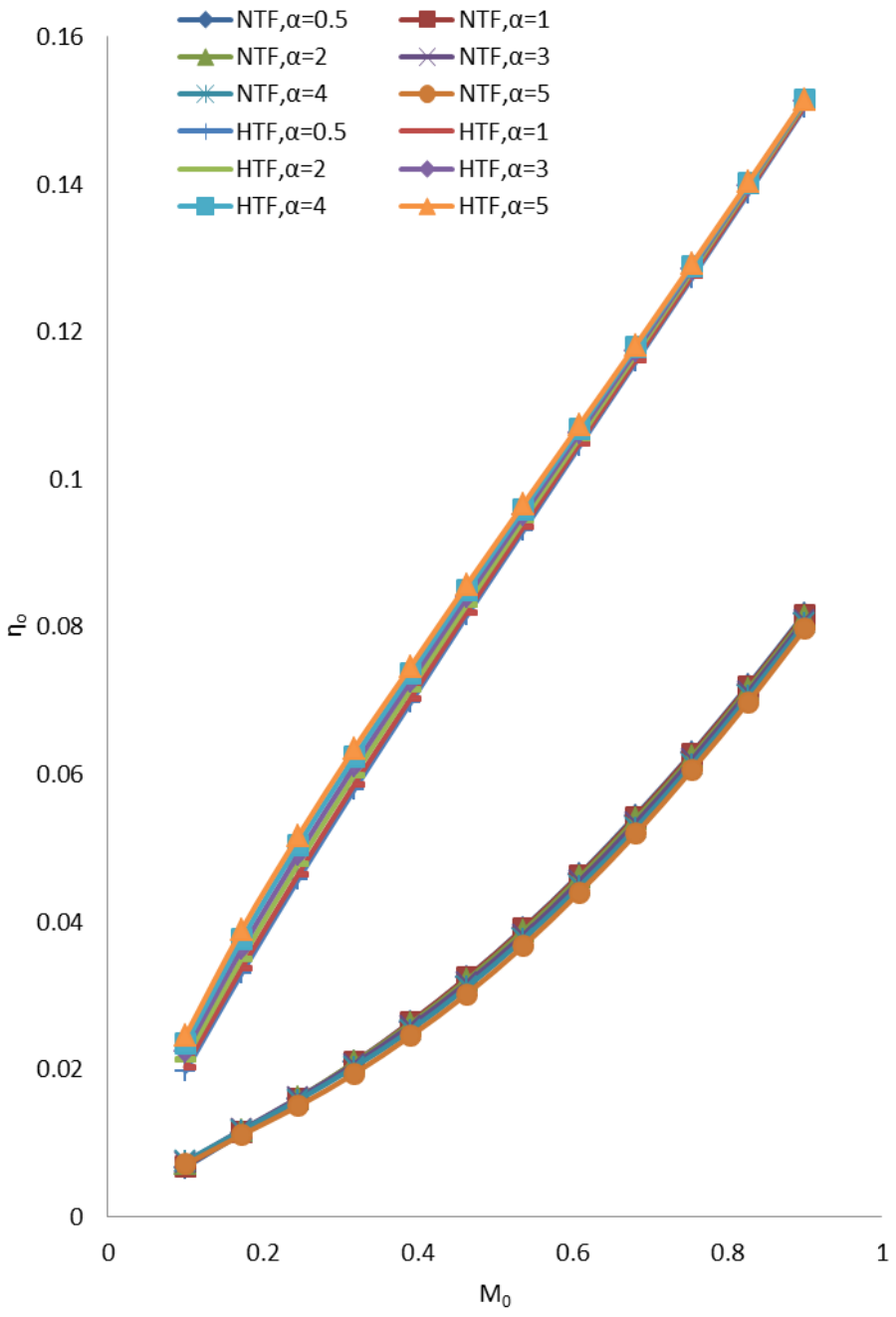

Figure 23 Comparison of performances of NTF and HTF versus M_0, for π_f=1.2 and π_c=1.5.Overall efficiency

Summary:

Figures 14 and 19 indicate that the specific thrust of a detonation-type turbofan is higher than that of a standard turbofan, irrespective of the parameter varied ($M_0, \pi_c, \alpha, \pi_f$). This is a positive outcome because high specific thrust is ideal for subsonic flight.

Figures 15 and 20 indicate that the thrust specific fuel consumption of a detonation-type turbofan is lower than that of a standard turbofan, irrespective of the parameter varied ($M_0, \pi_c, \alpha, \pi_f$). This is a positive outcome because low thrust specific fuel consumption implies lower fuel consumption per unit thrust generated.

Figures 16 and 21 indicate that the fuel air ratio of a detonation-type turbofan is lower than that of a standard turbofan, irrespective of the parameter varied (α, π_f) and is also independent of it.

Figures 17 and 22 indicate that the propulsive efficiency of a detonation-type turbofan is slightly lower than that of a standard turbofan, irrespective of the parameter varied ($M_0, \pi_c, \alpha, \pi_f$). Higher efficiencies are always desirable.

Figures 18 and 23 indicate that the overall efficiency of a detonation-type turbofan is higher than that of a standard turbofan, irrespective of the parameter varied ($M_0, \pi_c, \alpha, \pi_f$). Since overall efficiency is a product of thermal and propulsive efficiencies, and given the fact that propulsive efficiencies were only slightly higher it is can be said that HTFs have a reasonably good thermal efficiency which can be attributed to the detonation nature in its core.

CHAPTER 4

CONCLUSION AND FUTURE WORK

4.1 Advantages of the Integrated Turbofan

The Matlab code written is versatile and can be modified to analyze different types of air-breathing engines. The actual detonation-based TF has an improved performance over the conventional TF as shown in the results. This is attributed to the detonation process having a better thermal efficiency.

4.2 Disadvantages of the Integrated Turbofan

There can be a safety issue since we are dealing with detonations and very high pressure ratios. Thus further considerations are required compared to a standard turbofan. Since extremely high temperatures are produced inside the detonation chamber more new exotic alloys are required to withstand such temperatures which might not yet be available on a commercial scale.

4.3 Future Work

A more detailed performance analysis of the integrated TF will be done along with numerical simulation of the shock wave train inside of the constant area duct (isolator) and also of the detonation wave inside the detonation chamber. This will lead us to a better understanding of the practicality of detonations in real aircraft engines. Also more parameters will be included in the analysis and an off-design point performance analysis will be done in which more variation in the input parameters of the detonation chamber will be considered.

APPENDIX A

MATLAB CODE FOR HYBRID TURBOFAN ENGINE

```
function [F_mo,f,S,muuT,muuP,Muu0,muuC,Muut]=CDE_integrated_Turbofan
(M0,T0,gammac,Cpc,gammat,Cpt,Hpr,pidmax,pib,pin,pifn,ec,ef,et,muub,muun,P0_P9,P0_P19,
Tt4,pic,pif,alpha);
%%
% % sample syntax:
% % Turbofan ([1,2,3,4],2,3,4,5,6,7,8,9,1,2,4,5,3,6,7,8,9,1,2,3,4,5)
% % CDE_integrated_Turbofan
(M0,T0,gammac,Cpc,gammat,Cpt,Hpr,pidmax,pib,pin,pifn,ec,ef,et,muub,muun,P0_P9,P0_P19,
Tt4,pic,pif,alpha)
% % CDE_integrated_Turbofan
(.7,390,1.4,0.240,1.33,0.276,18400,0.99,0.96,0.99,0.99,0.90,0.89,0.89,0.99,0.99,0.9,0.9,3000,3
:.4167:8,2,.5)

clc;
clear taub
disp('Please enter the values of the input arguments as arrays of equal lengths.')

%%Air & H2%%%%%%%%%%

%% subscript 1 & 2 coresponds to the parameters before and after the TDW
%% respectively
%% Vectorizing

Y=ones(1,12);

if size(M0)<=1
   M0=M0*Y
else M0=M0
end

if size(T0)<=1
   T0=T0*Y;
else T0=T0
end

if size(gammac)<=1
   gammac=gammac*Y;
else gammac=gammac
end

if size(Cpc)<=1
   Cpc=Cpc*Y;
else Cpc=Cpc
end

if size(gammat)<=1
   gammat=gammat*Y;
else gammat=gammat
end
```

```
if size(Cpt)<=1
   Cpt=Cpt*Y;
else Cpt=Cpt
end

if size(Hpr)<=1
   Hpr=Hpr*Y;
else Hpr=Hpr
end

if size(pidmax)<=1
   pidmax=pidmax*Y;
else pidmax=pidmax
end

if size(pin)<=1
   pin=pin*Y;
else pin=pin
end

if size(pifn)<=1
   pifn=pifn*Y;
else pifn=pifn
end

if size(ec)<=1
   ec=ec*Y;
else ec=ec
end

if size(ef)<=1
   ef=ef*Y;
else ef=ef
end

if size(et)<=1
   et=et*Y;
else et=et
end

if size(muub)<=1
   muub=muub*Y;
else muub=muub
end

if size(muun)<=1
   muun=muun*Y;
else muun=muun
end
```

```
if size(P0_P9)<=1
   P0_P9=P0_P9*Y;
else P0_P9=P0_P9
end

if size(P0_P19)<=1
   P0_P19=P0_P19*Y;
else P0_P19=P0_P19
end

if size(pic)<=1
   pic=pic*Y;
else pic=pic
end

if size(pif)<=1
   pif=pif*Y;
else pif=pif
end

if size(alpha)<=1
   alpha=alpha*Y;
else alpha=alpha
end

%% deleting old values of pressure and temperature ratios

clear pib
clear Tt4

%% Determination of average temperature and pressure at station 4

% ContentsInput
% parameters %%
% Prandtl-Meyer function %%
% Determination of P,T as afunction of r %%
% Determination of average P,Ts %%

% Input parameters %%


h=.131; %% in metres %%
gamma_cj=1.242;
M_cj=4.3354;
radius=.218; %% in metres %%
C=2*pi*radius;
r=zeros*1000;%% vectorizing r
r=0.001:.01:C;
P_cj=1993371 ; %% in Pascals %%
T_cj= 2399.4 ; %% in Kelvin %%
```

```
%%

% Prandtl-Meyer function %%

muu_max=.5*((sqrt((gamma_cj+1)/(gamma_cj-1)))*atan(((gamma_cj-
1)/(gamma_cj+1))*(M_cj*M_cj-1))-atan(sqrt(M_cj^2-1)))

 for i=1:size(r,2)
    P_r(i)=P_cj*[(((1/gamma_cj)+((gamma_cj-1)/gamma_cj)*((C-
r(i))/C)))^(2*gamma_cj/(gamma_cj-1))]*[(h/(h+r(i)*sin(muu_max)))^gamma_cj];
    T_r(i)=T_cj*((P_r(i)/P_cj)^((gamma_cj-1)/gamma_cj));
 end

% subplot(2,1,1)
% plot (r,P_r,'.-b')
% xlabel('r')
% ylabel('P(r)')
% subplot(2,1,2)
% plot (r,T_r,'.-r')
% xlabel('r')
% ylabel('T(r)')

%%

% Determination of P,T as afunction of r %%

P_avg = sum(P_r)/size(r,2)
T_avg = sum(T_r)/size(r,2)

disp ('The above are the average exit pressure and temperature at station 4.')

%% calculation of M4,new Taub and pib %%

for i=1:1
M3=0.45;
gc=32.56;
T2=2399.4; %%%% in kelvin
a1=407.9; %% m/s local speed of sound ahead of the TDW
q2=1011.9;%% m/s local speed of sound behind of the TDW
a2=q2;
q1=537.9; % Absolute value of the velocity vector ahead the TDW
P1=  1.0e+006 * 0.2983; % input
P2=  1993371; %%% CEA o/p
T1=379.9197;% input
rho1=.8533;% density
rho2=4.6889; % from CEA
a=.0156;%(in metres)%width of self excited cell of the detonation front%%Taken from Bykovskii
lambda= 0.7* a;% (in metres)
h=12*a;% height of the combustible mixture layer
```

```
dc=40*lambda; % dia of the chamber
l=pi*dc; % distance between two TDWs
gamma1=1.4014;% from CEA
gamma2=1.1736;% from CEA
Cp=  1.0e+003 *[2.5817]; % From CEA
H0(i)=Cp(i)*T2(i)+ 0.5*q2(i)^2; % From Bykovskii: enthaply of the mixture components
Jo(i)=H0(i)+(gamma2(i)/(gamma2(i)-1))*573.41*T2(i);
v(i)=(2*(gamma2(i)-1)*Jo(i)/(gamma2(i)+1))^.5;% velocity in the axial direction
delta=.2 *h;% metres
k=0.15; %%% pure assumption based on nothing.
G1(i)=(1-k)*h*rho2(i)*q2(i)*delta; % h1*delta*rho2*q2
g(i)=G1(i)/(delta*l); % specific flow rate kg/s.m^2
rho(i)=g(i)/v(i); % density
P(i)=g(i)*v(i)/gamma2(i); %  Pressure at exit
M4(i)=v(i)/a2(i);

end
%% calculation of stagnation T & P at station 4

Tt3=T1*(1+(((gamma1-1)/2)*(M3^2)));
Pt3=P1*((1+(((gamma1-1)/2)*(M3^2)))^(gamma1/(gamma1-1)));
Tt4=T_avg*(1+(((gamma2-1)/2)*(M4(i)^2)));
Pt4=P_avg*((1+(((gamma2-1)/2)*(M4(i)^2)))^(gamma2/(gamma2-1)));

%% calcuation of the new Temperature and pressure ratios of the burner

taub=Tt4/Tt3;
pib=Pt4/Pt3;

%%

disp('taub')
taub'
disp('pib')
pib'
disp('Tt4')
Tt4'

if size(Tt4)<=1
   Tt4=Tt4*Y
else Tt4=Tt4
end

if size(pib)<=1
   pib=pib*Y
else pib=pib
end

%% Complete parametric analysis of the Hybrid TF after substituing the new
%% taub and pib
```

```
%%%%%%%%%%%%%%%%% JDMs nest%%%%%%%%%%%%%%%%%%%%
for i=1:12
Rc(i)=(gammac(i)-1)*Cpc(i)*778.16/gammac(i);
Rt(i)=(gammat(i)-1)*Cpt(i)*778.16/gammat(i);
a0(i)=sqrt(gammac(i)*Rc(i)*gc*T0(i));
taur(i)=1+(gammac(i)-1)*M0(i)*M0(i)/2;
pir(i)=taur(i)^(gammac(i)/(gammac(i)-1));
if    M0(i)<=1;
     muur(i)=1;
else  muur(i)=1-.0075*((M0(i)-1)^1.35);
end
pid(i)=pidmax(i)*muur(i);
taulambda(i)=(Cpt(i)*Tt4(i))/(Cpc(i)*T0(i));
tauc(i)=(pic(i))^((gammac(i)-1)/(gammac(i)*ec(i)));
muuc(i)=(pic(i)^((gammac(i)-1)/gammac(i))-1)/(tauc(i)-1);
tauf(i)=pif(i)^((gammac(i)-1)/(gammac(i)*ef(i)));
muuf(i)=((pif(i)^((gammac(i)-1)/(gammac(i))))-1)/(tauf(i)-1);
f(i)=(taulambda(i)-(taur(i)*tauc(i)))/(((muub(i)*Hpr(i))/(Cpc(i)*T0(i)))-taulambda(i));
taut(i)=1-((taur(i)/(muun(i)*(1+f(i))*taulambda(i)))*(tauc(i)-1+alpha(i)*(tauf(i)-1)));
pit(i)=(taut(i))^(gammat(i)/((gammat(i)-1)*et(i)));
muut(i)=(1-taut(i))/(1-taut(i)^(1/et(i)));
Pt9_P9(i)=(P0_P9(i))*pir(i)*pid(i)*pic(i)*pib(i)*pit(i)*pin(i);
M9(i)=sqrt((2/(gammat(i)-1))*(((Pt9_P9(i))^((gammat(i)-1)/gammat(i)))-1));
```

```
T9_T0(i)=(taulambda(i)*taut(i)*Cpc(i))/(((Pt9_P9(i))^((gammat(i)-1)/gammat(i)))*Cpt(i));

V9_a0(i)=M9(i)*sqrt((gammat(i)*Rt(i))/(gammac(i)*Rc(i))*(T9_T0(i)));

Pt19_P19(i)=(P0_P19(i))*pir(i)*pid(i)*pif(i)*pifn(i);

M19(i)=sqrt((2/(gammac(i)-1))*(((Pt19_P19(i))^((gammac(i)-1)/gammac(i)))-1));

T19_T0(i)=(taur(i)*tauf(i))/((Pt19_P19(i))^((gammac(i)-1)/gammac(i)));

V19_a0(i)=M19(i)*(T19_T0(i))^.5;

F_mo(i)=[(1/(1+alpha(i)))*(a0(i)/gc)*(((1+f(i))*V9_a0(i))-
M0(i)+((1+f(i))*((Rt(i)*T9_T0(i))/(Rc(i)*V9_a0(i)))*((1-
P0_P9(i))/gammac(i))))]+[(alpha(i)/(1+alpha(i)))*(a0(i)/gc)*(V19_a0(i)-
M0(i)+((T19_T0(i))/(V19_a0(i))*((1-P0_P19(i))/gammac(i))))];

S(i)=f(i)*3600/((1+alpha(i))*F_mo(i));

MuuP(i)=((2*M0(i)*(((1+f(i))*V9_a0(i))+(alpha(i)*V19_a0(i))-
(1+alpha(i))*M0(i))))/((1+f(i))*(V9_a0(i)^2)+(alpha(i)*(V19_a0(i))^2)-((1+alpha(i))*(M0(i)^2)));

MuuT(i)=(a0(i)^2)*((1+f(i))*(V9_a0(i))^2+alpha(i)*(V19_a0(i)^2)-
(1+alpha(i))*M0(i)^2)/(2*gc*f(i)*Hpr(i)*778.16);

MuuO(i)=MuuP(i)*MuuT(i);

end
%% Displaying output

disp('pid')
pid'
disp('taulambda')
taulambda'
disp('tauc')
tauc'
disp('muuc')
muuc'
disp('tauf')
tauf'
disp('taut')
taut'
disp('pit')
pit'
disp('muut')
muut'
disp('Pt9_P9')
Pt9_P9'
disp('M9')
```

```
M9'
disp('T9_T0')
T9_T0'
disp('V9_a0')
V9_a0'
disp('Pt19_P19')
Pt19_P19'
disp('M19')
M19'
disp('T19_T0')
T19_T0'
disp('V19_a0')
V19_a0'

disp('F_mo')
F_mo'
disp('S')
S'
disp('f')
f'
disp('MuuP')
MuuP'
disp('MuuO')
MuuO'
%% Plotting output

% figure,plot (pic,F_mo)
% xlabel('pic')
% ylabel('F_mo')
% figure,plot (pic,S)
% xlabel('pic')
% ylabel('S')
% % figure,plot (pic,MuuP)
% % xlabel('pic')
% % ylabel('muup')
% % figure,plot (pic,MuuO)
% % xlabel('pic')
% % ylabel('muuO')
%
% figure,plot (pif,F_mo)
% xlabel('pif')
% ylabel('F_mo')
% figure,plot (pif,S)
% xlabel('pif')
% ylabel('S')
% % figure,plot (pif,MuuO)
% % xlabel('pif')
% % ylabel('muuO')
% % figure,plot (pif,MuuP)
% % xlabel('pif')
% % ylabel('muup')
```

```
%
% figure,plot (M0,F_mo)
% xlabel('M0')
% ylabel('F_mo')
% figure,plot (M0,S)
% xlabel('M0')
% ylabel('S')
% figure,plot (M0,MuuP)
% xlabel('M0')
% ylabel('muup')
% figure,plot (M0,MuuO)
% xlabel('M0')
% ylabel('muuO')
```

APPENDIX B

MATLAB CODE FOR NORMAL TURBOFAN ENGINE

```
function [F_mo,f,S,muuT,muuP,Muu0,muuC,Muut]=Turbofan_Normal
(M0,T0,gammac,Cpc,gammat,Cpt,Hpr,pidmax,pib,pin,pifn,ec,ef,et,muub,muun,P0_P9,P0_P19,
Tt4,pic,pif,alpha);
%%
% % sample syntax:
% % Turbofan_Normal ([1,2,3,4],2,3,4,5,6,7,8,9,1,2,4,5,3,6,7,8,9,1,2,3,4,5)
% % Turbofan_Normal
(M0,T0,gammac,Cpc,gammat,Cpt,Hpr,pidmax,pib,pin,pifn,ec,ef,et,muub,muun,P0_P9,P0_P19,
Tt4,pic,pif,alpha)
% % Turbofan_Normal
(.7,390,1.4,0.240,1.33,0.276,18400,0.99,0.96,0.99,0.99,0.90,0.89,0.89,0.99,0.99,0.9,0.9,3000,3
:.4167:8,2,.5)

clc;
disp('Please enter the values of the input arguments as arrays of equal lengths.')

%%Air & H2%%%%%%%%%

%% subscript 1 & 2 coresponds to the parameters before and after the TDW
%% respectively
%% Vectorizing

Y=ones(1,12);

if size(M0)<=1
   M0=M0*Y
else M0=M0
end

if size(T0)<=1
   T0=T0*Y;
else T0=T0
end

if size(gammac)<=1
   gammac=gammac*Y;
else gammac=gammac
end

if size(Cpc)<=1
   Cpc=Cpc*Y;
else Cpc=Cpc
end

if size(gammat)<=1
   gammat=gammat*Y;
else gammat=gammat
end

if size(Cpt)<=1
```

```
    Cpt=Cpt*Y;
else Cpt=Cpt
end

if size(Hpr)<=1
    Hpr=Hpr*Y;
else Hpr=Hpr
end

if size(pidmax)<=1
    pidmax=pidmax*Y;
else pidmax=pidmax
end

if size(pin)<=1
    pin=pin*Y;
else pin=pin
end

if size(pifn)<=1
    pifn=pifn*Y;
else pifn=pifn
end

if size(ec)<=1
    ec=ec*Y;
else ec=ec
end

if size(ef)<=1
    ef=ef*Y;
else ef=ef
end

if size(et)<=1
    et=et*Y;
else et=et
end

if size(muub)<=1
    muub=muub*Y;
else muub=muub
end

if size(muun)<=1
    muun=muun*Y;
else muun=muun
end

if size(P0_P9)<=1
```

```
    P0_P9=P0_P9*Y;
else P0_P9=P0_P9
end

if size(P0_P19)<=1
    P0_P19=P0_P19*Y;
else P0_P19=P0_P19
end

if size(pic)<=1
    pic=pic*Y;
else pic=pic
end

if size(pif)<=1
    pif=pif*Y;
else pif=pif
end

if size(alpha)<=1
    alpha=alpha*Y;
else alpha=alpha
end
if size(Tt4)<=1
    Tt4=Tt4*Y
else Tt4=Tt4
end

if size(pib)<=1
    pib=pib*Y
else pib=pib
end
gc=32.56;

%% Complete parametric analysis of the normal TF


%%%%%%%%%%%%%%%%% JDMs nest%%%%%%%%%%%%%%%%%%%%

for i=1:12

Rc(i)=(gammac(i)-1)*Cpc(i)*778.16/gammac(i);

Rt(i)=(gammat(i)-1)*Cpt(i)*778.16/gammat(i);

a0(i)=sqrt(gammac(i)*Rc(i)*gc*T0(i));

taur(i)=1+(gammac(i)-1)*M0(i)*M0(i)/2;
```

```
pir(i)=taur(i)^(gammac(i)/(gammac(i)-1));
if    M0(i)<=1;
      muur(i)=1;
else  muur(i)=1-.0075*((M0(i)-1)^1.35);
end
pid(i)=pidmax(i)*muur(i);
taulambda(i)=(Cpt(i)*Tt4(i))/(Cpc(i)*T0(i));
tauc(i)=(pic(i))^((gammac(i)-1)/(gammac(i)*ec(i)));
muuc(i)=(pic(i)^((gammac(i)-1)/gammac(i))-1)/(tauc(i)-1);
tauf(i)=pif(i)^((gammac(i)-1)/(gammac(i)*ef(i)));
muuf(i)=((pif(i)^((gammac(i)-1)/(gammac(i))))-1)/(tauf(i)-1);
f(i)=(taulambda(i)-(taur(i)*tauc(i)))/(((muub(i)*Hpr(i))/(Cpc(i)*T0(i)))-taulambda(i));
taut(i)=1-((taur(i)/(muun(i)*(1+f(i))*taulambda(i)))*(tauc(i)-1+alpha(i)*(tauf(i)-1)));
pit(i)=(taut(i))^(gammat(i)/((gammat(i)-1)*et(i)));
muut(i)=(1-taut(i))/(1-taut(i)^(1/et(i)));
Pt9_P9(i)=(P0_P9(i))*pir(i)*pid(i)*pic(i)*pib(i)*pit(i)*pin(i);
M9(i)=sqrt((2/(gammat(i)-1))*(((Pt9_P9(i))^((gammat(i)-1)/gammat(i)))-1));
T9_T0(i)=(taulambda(i)*taut(i)*Cpc(i))/(((Pt9_P9(i))^((gammat(i)-1)/gammat(i)))*Cpt(i));
V9_a0(i)=M9(i)*sqrt((gammat(i)*Rt(i))/(gammac(i)*Rc(i))*(T9_T0(i)));
Pt19_P19(i)=(P0_P19(i))*pir(i)*pid(i)*pif(i)*pifn(i);
M19(i)=sqrt((2/(gammac(i)-1))*(((Pt19_P19(i))^((gammac(i)-1)/gammac(i)))-1));
T19_T0(i)=(taur(i)*tauf(i))/((Pt19_P19(i))^((gammac(i)-1)/gammac(i)));
V19_a0(i)=M19(i)*(T19_T0(i))^.5;
```

```
F_mo(i)=[(1/(1+alpha(i)))*(a0(i)/gc)*(((1+f(i))*V9_a0(i))-
M0(i)+((1+f(i))*((Rt(i)*T9_T0(i))/(Rc(i)*V9_a0(i)))*((1-
P0_P9(i))/gammac(i))))]+[(alpha(i)/(1+alpha(i)))*(a0(i)/gc)*(V19_a0(i)-
M0(i)+((T19_T0(i))/(V19_a0(i))*((1-P0_P19(i))/gammac(i))))];

S(i)=f(i)*3600/((1+alpha(i))*F_mo(i));

MuuP(i)=((2*M0(i)*(((1+f(i))*V9_a0(i))+(alpha(i)*V19_a0(i))-
(1+alpha(i))*M0(i))))/((1+f(i))*(V9_a0(i)^2)+(alpha(i)*(V19_a0(i))^2)-((1+alpha(i))*(M0(i)^2)));

MuuT(i)=(a0(i)^2)*((1+f(i))*(V9_a0(i))^2+alpha(i)*(V19_a0(i)^2)-
(1+alpha(i))*M0(i)^2)/(2*gc*f(i)*Hpr(i)*778.16);

MuuO(i)=MuuP(i)*MuuT(i);

end
%% Displaying output

disp('pid')
pid'
disp('taulambda')
taulambda'
disp('tauc')
tauc'
disp('muuc')
muuc'
disp('tauf')
tauf'
disp('taut')
taut'
disp('pit')
pit'
disp('muut')
muut'
disp('Pt9_P9')
Pt9_P9'
disp('M9')
M9'
disp('T9_T0')
T9_T0'
disp('V9_a0')
V9_a0'
disp('Pt19_P19')
Pt19_P19'
disp('M19')
M19'
disp('T19_T0')
T19_T0'
disp('V19_a0')
V19_a0'
disp('F_mo')
```

```
F_mo'
disp('S')
S'
disp('f')

f'

disp('MuuP')

MuuP'

disp('MuuO')

MuuO'
```

APPENDIX C

CEA INPUT AND OUTPUT

pif=2, M0=0.7, all pressures in (Bars).

pic	tauc	tauf	γ	M3	P0	T0(K)	P3	T3(K)	γ_cj	M_cj	D(m/s)	P_cj	T_cj(K)	a2(m/s)
1.2	1.0534	1.0534	1.4	0.5	1.013	300	1.706	348	1.165	4.487	1970	22.891	2987.72	1098.1
1.3	1.0778	1.0534	1.4	0.5	1.013	300	1.848	356.21	1.166	4.438	1970.7	24.249	2994.72	1099.5
1.4	1.1009	1.0534	1.4	0.5	1.013	300	1.990	363.83	1.165	4.394	1971.5	25.712	3001.64	1100.8
1.5	1.1228	1.0534	1.4	0.5	1.013	300	2.132	371.08	1.166	4.353	1972.1	27.041	3007.87	1102.1
1.6	1.1437	1.0534	1.4	0.5	1.013	300	2.274	377.98	1.167	4.314	1972.7	28.28	3013.62	1103.2
1.8	1.1828	1.0534	1.4	0.5	1.013	300	2.559	390.92	1.167	4.246	1973.8	30.91	3024.66	1105.4
1.9	1.2012	1.0534	1.4	0.5	1.013	300	2.701	397.01	1.167	4.215	1974.3	32.144	3029.7	1106.4
2.0	1.2190	1.0534	1.4	0.5	1.013	300	2.843	402.87	1.168	4.185	1974.8	33.386	3034.57	1107.4
2.2	1.2526	1.0534	1.4	0.5	1.013	300	3.127	413.99	1.168	4.133	1975.6	35.715	3043.52	1109.2
2.3	1.2686	1.0534	1.4	0.5	1.013	300	3.270	419.28	1.168	4.107	1976.1	36.992	3048	1110.1
2.4	1.2841	1.0534	1.4	0.5	1.013	300	3.412	424.41	1.168	4.083	1976.4	38.139	3052.11	1110.9

REFERENCES

[1] Mattingly, J. M. (2005). *Elements of Gas Turbine Propulsion.* AIAA education series.

[2] Kuo, K. K. (1986). *Principles of Combustion.* Pennsylvania: John Wiley and Sons.

[3] Bykovskii, F. A., Zhdan, S. A., & Vedenikov, E. F. (2006). Contionous Spin Detonations. *Journal of Propulsion and Power*.

[4] Braun, E. M., Wilson, D. R., Camberos, A. J., & Lu, F. K. (July 25-28, 2010). Detonation Engine Performance Comparison Using First and Second Law analysis. *46th AIAA/ASME/SAE/ASEE Joint Propulsion conference & Exhibit.* Nashville, Tennessee: AIAA.

[5] Anderson, J. D. (2002). *Modern Compressible Flow* (3 ed.). McGraw Hill.

[6] Gere, J. M., & Timoshenko, S. P. (1997). *Mechanics of Materials.* PWS Publishing Company.

[7] Braun, E. M., Lu, F. K., Wilson, D. R., & Camberos, J. A. (July 25-28,2010). Air Breathing Rotating Detonation Waave Engine Cycle Analysis. *46th AIAA/ASME/SAE/ASEE Joint Propulsion Conferene and Exhibit.* NAshville, Tennessee: AIAA .

[8] *Fluent Manual 10.0.* Fluent.

[9] Vasil'ev, A. A., & Nikolev, Y. A. (1978). Closed Theoretical Model of a Detonation Cell. *Acta Astronautica, 5*, 983-996.

[10] *NASA RO-1311 User Manual part-1.* NASA.

[11] *CEA*. Retrieved from http://www.grc.nasa.gov/WWW/CEAWeb/ceaHome.ht

[12] Heiser, W. H., & Pratt, D. D. (1994). *Hypersonic Air Breathing Propulsion.* Washington, DC: AIAA series.

BIOGRAPHICAL INFORMATION

Yashwanth M. Swamy was born in Bangalore, India in February 1986. He attended M.S.Ramaiah Institute of Technology, Bangalore, where he received his Bachelors in Mechanical Engineering in 2008. He joined University of Texas at Arlington in 2009 to pursue his Master of Science in Aerospace Engineering. His interests include Propulsion, Computational Fluid Dynamics and Gas dynamics.